Cortical fibers orientation mapping using in-vivo whole brain 7 T diffusion MRI

NeuroImage 178 (2018) 104–118

Contents lists available at ScienceDirect

NeuroImage

journal homepage: www.elsevier.com/locate/neuroimage

Cortical fibers orientation mapping using in-vivo whole brain 7 T diffusion MRI

Omer F. Gulban [a], Federico De Martino [a], An T. Vu [b], Essa Yacoub [c], Kamil Uğurbil [c], Christophe Lenglet [c,*]

[a] Department of Cognitive Neuroscience, Maastricht University, Maastricht, Netherlands
[b] Veterans Affairs Health Care System, San Francisco, CA, USA
[c] Center for Magnetic Resonance Research, University of Minnesota, Minneapolis, MN, USA

ARTICLE INFO

Keywords:
Diffusion MRI
7 T
High resolution
Cortex
Depth dependent analysis
Gyral bias

ABSTRACT

Diffusion MRI of the cortical gray matter is challenging because the micro-environment probed by water molecules is much more complex than within the white matter. High spatial and angular resolutions are therefore necessary to uncover anisotropic diffusion patterns and laminar structures, which provide complementary (e.g. to anatomical and functional MRI) microstructural information about the cortex architectonic. Several *ex-vivo* and *in-vivo* MRI studies have recently addressed this question, however predominantly with an emphasis on specific cortical areas. There is currently no *whole brain in-vivo* data leveraging multi-shell diffusion MRI acquisition at high spatial resolution, and depth dependent analysis, to characterize the complex organization of cortical fibers. Here, we present unique *in-vivo* human 7T diffusion MRI data, and a dedicated cortical depth dependent analysis pipeline. We leverage the high spatial (1.05 mm isotropic) and angular (198 diffusion gradient directions) resolution of this whole brain dataset to improve cortical fiber orientations mapping, and study neurites (axons and/or dendrites) trajectories across cortical depths. Tangential fibers in superficial cortical depths and crossing fiber configurations in deep cortical depths are identified. Fibers gradually inserting into the gyral walls are visualized, which contributes to mitigating the gyral bias effect. Quantitative radiality maps and histograms in individual subjects and cortex-based aligned datasets further support our results.

Introduction

Diffusion MRI (dMRI) relies on the anisotropic diffusion of water molecules, hindered by barriers such as axonal membranes and myelin (Beaulieu, 2002), to produce three-dimensional images which characterize the microstructure of nervous tissue. Acquisition techniques, such as diffusion tensor imaging (Basser et al., 1994), high angular resolution diffusion imaging (Tuch et al., 2002), diffusion spectrum imaging (Wedeen et al., 2005) and more recent methods sensitive to axonal density and size (Assaf and Basser, 2005; Alexander et al., 2010; Zhang et al., 2012; Farooq et al., 2016), have been introduced to investigate the organization of axonal fibers. However, the vast majority of *in-vivo* dMRI studies have focused on the white matter so far, with recent advances (Lenglet et al., 2009; Sotiropoulos et al., 2013) enabling the exploration of connectivity patterns between cortical and subcortical brain areas. Despite these formidable developments, there are still many limitations related to the ability of dMRI data to disentangle complex white matter fiber configurations (Seunarine and Alexander, 2014; Thomas et al., 2014). The Human Connectome Project (HCP) (Van Essen et al., 2012, 2013) has recently made significant strides in this direction, to map macroscopic structural and functional connectivity patterns of the human brain using 3 T (3T) and 7 T (7T) MRI (Smith et al., 2013; Sotiropoulos et al., 2013; Vu et al., 2015, 2017).

Using HCP data and a semi-automated neuroanatomical analysis method, Glasser et al. (2016) successfully identified 97 new areas per hemisphere based on their cortical (myelo-) architecture and functional connectivity. Such work, along with other *in-vivo* MRI investigations (Geyer et al., 2011; Barazany and Assaf, 2012; Dick et al., 2012; Deistung et al., 2013; Nagy et al., 2013; Lutti et al., 2014; De Martino et al., 2015; Dinse et al., 2015; Helbling et al., 2015; Zhang et al., 2015; Waehnert et al., 2016; Trampel et al., 2017) and a recent collection of review papers (Turner and Geyer, 2014), is opening new avenues towards achieving "*in-vivo* histology". Adding microstructural information about the cortical gray matter, obtained with dMRI, would provide complementary

* Corresponding author.
E-mail address: clenglet@umn.edu (C. Lenglet).

https://doi.org/10.1016/j.neuroimage.2018.05.010
Received 18 December 2017; Received in revised form 28 March 2018; Accepted 2 May 2018
Available online 10 May 2018

details about the cortex cyto- and myelo-architectonics (Eickhoff et al., 2005), and likely further improve those cortical parcellations (Nagy et al., 2013). However, dMRI of the cortex is particularly challenging because neuronal cell bodies and dendrites, in addition to axons, render the micro-environments probed by water molecules much more complex than in the white matter. As a result, diffusion quantified by dMRI appears more isotropic (with fractional anisotropy below 0.25), especially at low spatial resolutions. In this paper, we aim to demonstrate that 7T whole brain and high resolution dMRI, along with a customized analysis, can provide exquisite insights into the organization of fibers in the human cerebral cortex.

The cortex follows a laminar organization (Baillarger, 1840; Vogt, 1903; Vogt and Vogt, 1919), as illustrated on Fig. 1, which varies across cortical areas. For instance, the primary visual cortex is uniquely characterized by the band of Gennari (or outer band of Baillarger), which constitutes the only formation of transverse myelinated fibers visible to the naked eye. Cortical fibers are essentially oriented in a radial or tangential (transverse) fashion, with the later type of fibers existing in layers I, IV, V and VI of all cortical areas (Peters and Sethares, 1996; Nieuwenhuys, 2013). Fig. 1 summarizes the cyto- and myelo-architectonic properties of the six layers of the cortex. Layer I (molecular layer) mostly contains dendrites from pyramidal neurons and tangential myelinated fiber constituting the plexus of Exner. Layer II (external granular layer) mostly contains cells bodies and few fibers. Layer III (external pyramidal layer) mostly contains small pyramidal neurons as well as radial intra-cortical fibers. Layer IV (internal granular layer) contains pyramidal and stellate neurons receiving thalamic and intra-hemispheric cortical input. It also contains a set of dense tangential fibers: the outer band of Baillarger. Layer V (internal pyramidal layer) contains large pyramidal neurons with radial axons projecting to subcortical areas. It also contains another set of dense tangential fibers: the inner band of Baillarger. Layer VI contains small pyramidal and multiform cells, with projections to the thalamus. The deeper section of layer VI (closer to the white matter) contains more tangential fibers (Vandevelde et al., 1996). In addition to the radial axons present in layers II, III, IV, V and VI, radial apical dendrites originating from the pyramidal cells also exist (Peters and Sethares, 1996). Tangential crossing fibers in layers I, IV-VI have been observed *ex-vivo* (Van Essen et al., 1986), including with dMRI (Kleinnijenhuis et al., 2013; Leuze et al., 2014; Aggarwal et al., 2015), but they remain particularly challenging to observe *in-vivo*.

There are only a handful of dMRI studies on cortical anisotropy and fiber orientations mapping. To the best of our knowledge, so far, imaging studies, whether *ex-vivo* (McNab et al., 2009; Miller et al., 2011; Dell'Acqua et al., 2013; Kleinnijenhuis et al., 2013; Leuze et al., 2014; Aggarwal et al., 2015; Bastiani et al., 2016), or *in-vivo* (Jaermann et al., 2008; Anwander et al., 2010; Heidemann et al., 2010; McNab et al., 2013; Truong et al., 2014; Kleinnijenhuis et al., 2015), have exclusively focused on specific cortical areas (e.g., motor, visual), with the exception of (Anwander et al., 2010; Kang et al., 2012; Nagy et al., 2013; Fan et al., 2017) and (McNab et al., 2009; Miller et al., 2011), which acquired whole-brain data.

Ex-vivo data at very high spatial resolution (100–300 μm) have successfully demonstrated the laminar organization of the cortex, with distinct radial and tangential diffusion properties and layer dependence of anisotropy, for example in post-mortem brain blocks from the visual cortex (Kleinnijenhuis et al., 2013; Leuze et al., 2014). Lower anisotropy was found in the bands of Baillarger and deeper cortical layers, due to complex fiber configurations resulting from the intersection of radial (pyramidal) and tangential cortico-cortical fibers. Using high angular resolution diffusion imaging (HARDI), a few *ex-vivo* studies (Kleinnijenhuis et al., 2013; Leuze et al., 2014; Aggarwal et al., 2015) have successfully reconstructed such complex fiber orientation in layers I, IV-V and VI.

In-vivo data have predominantly supported radial fiber orientations, perpendicular to the gray matter/white matter (GM/WM) interface.

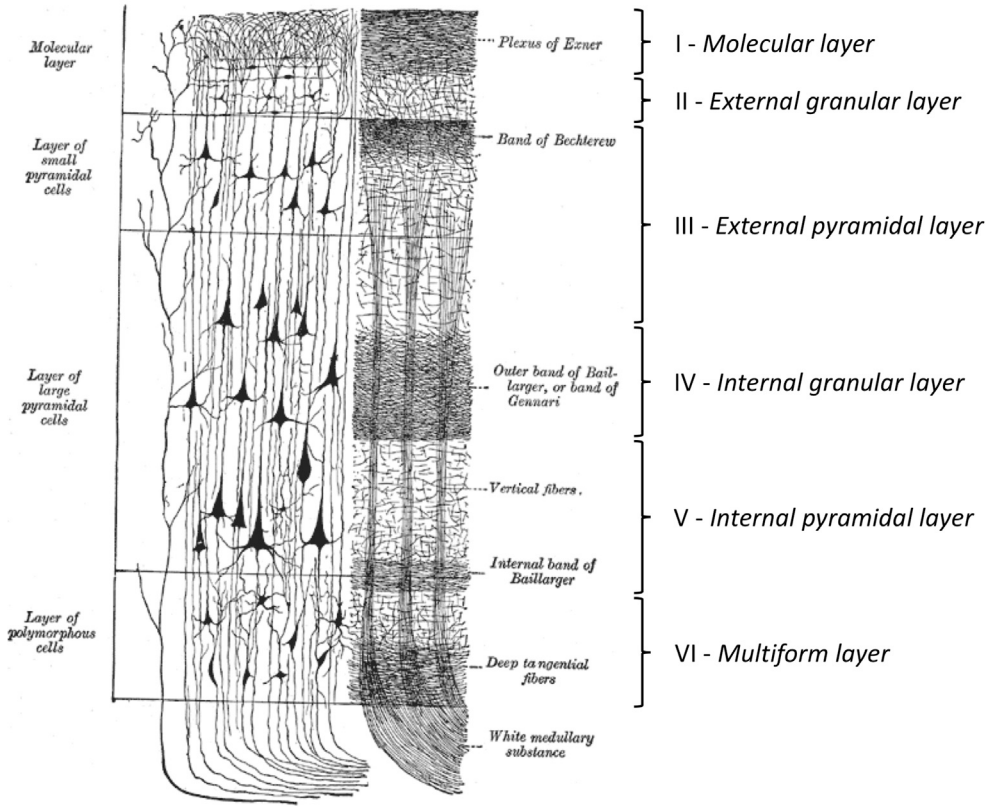

Fig. 1. Cyto-architectonic (left) and myelo-architectonic (right) organization of the human cerebral cortex. Adapted from *H. Gray. Anatomy of the Human Body, 1918. Plate 754* (public domain).

Specifically, radial fibers presumably related to pyramidal cells of layer V, such as the cells of Betz (Braak and Braak, 1976; Ramaswamy and Markram, 2015), were identified in the motor and prefrontal cortex, while tangential fibers appeared in somatosensory and parietal cortices (Anwander et al., 2010). Interestingly, these observations were made in the gyri and sulcal walls but no specific orientation pattern was detected in sulcal fundi, possibly because of the relatively low spatial resolution (1.5 mm isotropic). Those findings were recently expanded upon, using a surface-based and cortical depth dependent analysis method (McNab et al., 2013), to confirm transition from radial to tangential diffusion tensor orientation between the motor and somatosensory cortices. In addition, their data supported similar orientation patterns in the middle cortical depth of the somatosensory cortex. Interestingly, histograms of radiality distribution in the gyri, sulcal walls and sulcal fundi of the pre-/post-central, supra-marginal and transverse-temporal cortices did not show significant differences, with most locations exhibiting radial orientation.

Dependence of anisotropy on cortical depth was recently demonstrated *in-vivo* (Kang et al., 2012; Truong et al., 2014), with lower values in the upper and lower depths. Contrary to *ex-vivo* data, reduced anisotropy was not reported in the middle depths (presumably related to the bands of Baillarger), possibly because of the lower resolution of *in-vivo* data. In addition, only a weak correlation between fiber orientation and anisotropy was found in the middle depths of several cortical areas (McNab et al., 2013). Finally, although earlier data (McNab et al., 2013) did not appear to support dependence of fiber orientation with the cortical surface curvature, more recent results have shown that diffusivity, anisotropy and fiber orientation do appear to differ in the gyral crowns, sulcal walls and fundi (Sotiropoulos et al., 2016), with radiality being maximal in the middle cortical depth next to the gyral crowns, consistent with high anisotropy, and being minimal in deeper gray matter in sulcal fundi (Kleinnijenhuis et al., 2015; Fan et al., 2017).

Recent work (Nie et al., 2012; Chen et al., 2013; Van Essen et al., 2014) about cortical tractography has illustrated the tendency of such approaches to predominantly terminate in the gyral crowns and less often reach the sulcal fundi. The magnitude of this bias has been shown to be in the order *x*40 for *in-vivo* human dMRI and *x*180 for *ex-vivo* non-human primate dMRI. However, this so-called "gyral bias" has not been observed in anatomical retrograde or anterograde tracer studies (Van Essen et al., 2014) and it is known that projections to specific cortical areas are broadly distributed in gyri and sulci (Markov et al., 2011, 2014). This artefactual bias is therefore likely explained by a combination of technical limitations of current dMRI data and analysis methods. In particular, the massive dominance of estimated fibers pointing directly toward the gyral crown in and near the WM forces tractography to converge to gyri.

Moreover, understanding the organization of axonal fibers in and near the cortex is crucial and still largely unexplored. Histological data (Van Essen et al., 1986, 2014) demonstrated that, although many axons run from the deep WM into the gyral crown with little curvature, many axonal trajectories also curve at oblique angles into the cortex and through the gyral wall, before becoming radial. This is illustrated in Fig. 2. Near sulcal fundi, fibers configuration is very different, with a large number of tangential orientations and sharper turns (compared to gyral walls) into the cortex. Although some *ex-vivo* dMRI data have shown good agreement at and near the GM/WM interface, there is very little *in-vivo* data – let alone whole brain – to investigate axonal fibers pattern in and near the cortex. It is therefore imperative to design acquisition and dedicated analysis methods to investigate the microstructure of the complete human cerebral cortex *in-vivo*. Here, we use an *in-vivo* imaging protocol based on the 7T HCP dMRI protocol (Vu et al., 2015), extended to a high maximum *b*-value of 3000 s/mm^2, and obtained within approximately the same time as the 3T HCP dMRI data (e.g. 1 h) to which our results are compared. We analyze the datasets with a dedicated cortical depth dependent method (Kemper et al., 2017). Our analysis strategy defines three cortical depths relative to the local cortical thickness, and thus relates to the actual layered organization of the cortex only as a down-sampled approximation. Nevertheless, the combination of such data and analysis enables to investigate the organization of axonal trajectories within the cortex, *in-vivo* and across cortical depths.

We present *whole brain in-vivo* data leveraging multi-shell HARDI acquisition with 1.05 mm isotropic spatial resolution to characterize complex fibers organization in superficial, middle and deep cortical depths, relative to the local gray matter thickness. The employed cortical depth dependent analysis enables full utilization of the richness of such datasets. Moreover, as noted above, we highlighted several differences among *in-vivo* results (e.g., dependence of fiber orientation on cortical surface curvature), and, more importantly between *in-vivo* and *ex-vivo* dMRI data; we hypothesize that these discrepancies are due to insufficient spatial and angular resolution of *in-vivo* data. Recent work on the organization of fibers in and around the human cortex using dMRI has shown improved detection of fibers perpendicular to the gyral walls and sulcal fundi, for example by combining 3T and 7T dMRI data (Sotiropoulos et al., 2016), or by combining data with low spatial resolution and high *b*-value (optimal for white matter fiber crossings detection) and data with high spatial resolution and low *b*-value (Fan et al., 2017). Here, we demonstrate that the higher spatial resolution attainable with dMRI at 7T (compared to 3T) reduces the impact of the gyral bias and results in more neuroanatomically plausible results.

Material and methods

MRI acquisitions

We acquired whole brain dMRI data at Maastricht University in N = 6 healthy volunteers using a 7T Siemens MAGNETOM scanner, with 70 mT/m gradients and a 32-channel receive coil (Nova Medical). We extended the 7T HCP protocol (Vu et al., 2015), which utilizes two shells (*b*-values = 1000 and 2000 s/mm^2), with an additional shell at *b* = 3000 s/mm^2. The final parameters employed were: Field-of-view 200 × 200 with partial Fourier 6/8, 132 slices, nominal voxel size = 1.05 mm isotropic, TR/TE = 7080/75.6 ms, MB = 2, phase

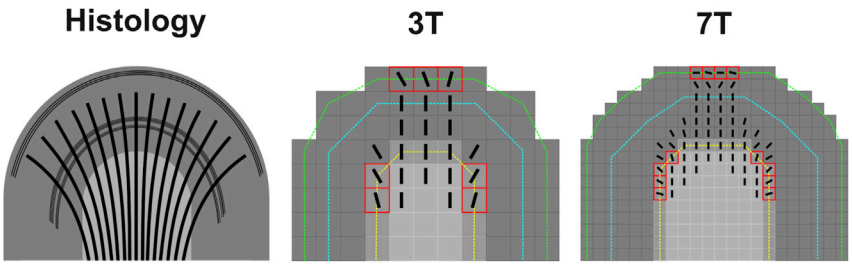

Fig. 2. Illustration of the gyral bias issue. While axons emanating from the white matter progressively insert into the cortex, tractography algorithms tend to follow the dominant fiber orientation and mostly capture connections ending in the gyral crown. This effect is compounded by limitations related to the spatial resolution of diffusion MRI data. This may be mitigated, to some extent, with improved reconstruction of fiber orientations using high resolution 7T dMRI.

encoding acceleration (GRAPPA) = 3, *b*-values = 1000, 2000, 3000 s/mm^2, 66 directions and 11 additional $b = 0$ vol per *b*-value. A total of 462 vol were obtained (231 in each phase encoding direction AP and PA) for a total acquisition time of 60 min. T_1-and PD-weighted anatomical scans (voxel size = 0.7 mm^3 isotropic) were also obtained in each subject. The study was approved by the Maastricht University ethics committee, and written informed consent was obtained from all participants.

For comparison, pre-processed 3 T dMRI datasets (Open Access) from the HCP ConnectomeDB database[1] (Sotiropoulos et al., 2013; Van Essen et al., 2013) from N = 6 healthy unrelated volunteers were also analyzed. The subjects for the 7T and 3T datasets were not the same. The 3T HCP datasets were acquired using the 3T Siemens Connectome Skyra scanner with 100 mT/m gradients and a 32-channel receive coil (Ugurbil et al., 2013). The following parameters were used: Field of view 144 × 168 with partial Fourier 6/8, 111 slices, nominal voxel size = 1.25 mm isotropic, TR/TE = 5500/89 ms, MB = 3, no in-plane acceleration, *b*-values = 1000, 2000, 3000 s/mm^2, 90 directions and 5 additional $b = 0$ vol per *b*-value. A total of 570 vol were obtained (285 in each phase encoding direction LR and RL) for a total acquisition time of 60 min.

We point out, as noted in previous work (Sotiropoulos et al., 2016), that the seemingly small difference in nominal voxel size (1.25 mm vs. 1.05 mm isotropic) leads to a reduction of the voxel volume by 40%. Additionally, point spread function blurring in the phase encoding direction (AP at 7T and LR at 3T) is reduced at 7T with the use of in-plane acceleration, thereby further increasing the gain in spatial resolution (Vu et al., 2015). Each dataset is unprecedented in its own right, as far as *in-vivo* human diffusion imaging is concerned, as illustrated in Fig. 3.

Despite some degree of signal loss in the lower parts of the brain (inferior temporal areas, Fig. 3), due to the well-known B_1 penetration problems at 300 MHz radiofrequency (Ugurbil, 2014; Wu et al., 2017), it can be seen that the 7T data provides exquisite details in the rest of the brain, including a visible dark band of low fractional anisotropy (white arrow in Fig. 3A) in the deeper cortical depths. This finding has been reported in *in-vivo* cat (Ronen et al., 2005) or primate and human *ex-vivo* studies (D'Arceuil et al., 2007; McNab et al., 2009; Miller et al., 2011). It has been putatively attributed to either a sharp transition of the fiber directions as they enter the cortex, especially in sulcal walls and fundi, or tangential fibers from layers V-VI, crossing with radial axonal projections from pyramidal neurons. Fig. 3B illustrates the organization of this band of low FA in the right superior frontal gyrus for one of our 7T datasets. It can be clearly seen that the dark band runs continuously along the sulcal walls and fundus, but is much less evident in the gyral crown, consistent with fibers entering gyri radially, with minimal curvature. We will also present results supporting the hypothesis of crossing fibers as a potential explanation for the presence of this low FA band in the deeper cortical depths. This possible explanation was recently described elsewhere (Kleinnijenhuis et al., 2013), based on an *ex-vivo* study where the authors successfully identified the inner and outer band of Baillarger in the human primary visual cortex. They noted that the inner band can sometimes appear continuous with layer VI and the WM (Baillarger, 1840). Given the resolution of our data, it is likely that we also observe this phenomenon, with layers V and VI contributing to crossing fiber configurations in the deeper cortical depths and therefore leading to reduced FA. We also did not observe the outer band of Baillarger (band of Gennari) in our data.

Data analysis

Distortion and motion correction: dMRI data was corrected for distortions with the HCP pipeline (Glasser et al., 2013; Sotiropoulos et al., 2013). Specifically, geometric and eddy-current distortions, as well as head motion, were corrected by modeling and combining data acquired with opposite phase encoding directions (Andersson et al., 2003; Andersson and Sotiropoulos, 2015, 2016).

Fiber orientation mapping and tractography: Fiber orientations were estimated voxel by voxel using either the diffusion tensor model (DTI) (Basser et al., 1994) or the "ball & stick" fiber orientation density (fODF) model with up to three possible fiber compartments (in addition to the isotropic diffusion compartment) (Behrens et al., 2007). In order to account for the non mono-exponential decay of the multi-shell diffusion signal, we used an extension of the "ball & stick" model (Jbabdi et al., 2012). Fiber orientations estimation was performed using the "BedpostX" module of the FMRIB Software Library Diffusion Toolbox version 3.0 (Jenkinson et al., 2012). Tractography was performed within masks of the motor cortex (M1 and S1), defined manually, using the implementation in DSI Studio[2] of a generalized DTI deterministic tracking algorithm (Yeh et al., 2013) with the following parameters: FA threshold = 0.05, angular threshold = 90, step size = 0.20 mm, smoothing weight = 0.2, minimum/maximum tract length = 5/50 mm, fiber orientation interpolation: Gaussian radial basis, tracking algorithm: Euler, and number of reconstructed tracts = 10,000. Trackvis[3] is used for visualization (Figs. 7 and 8).

Cortical depth dependent analysis

For the 7T data, analysis of anatomical scans, and delineation of the inner (GM/WM) and outer (pial) gray matter surfaces (e.g. Fig. 4) was conducted from unbiased (normalized by proton density) T_1-weighted images (Van de Moortele et al., 2009) up-sampled to a spatial resolution of 0.5 mm^3 isotropic (Kemper et al., 2017). The delineation of the same surfaces (inner and outer gray matter) for the 3T HCP data was based on the results from the HCP pipeline (Glasser et al., 2013). For the 7T data, using cortical thickness, we estimated a surface half-way between the GM/WM interface and pial surface for each subject and hemisphere. This surface was sampled on a homogenous sphere to perform cortex based alignment (Goebel et al., 2006). This information (i.e. the vertex to vertex correspondence across subjects) was used to create group maps of fibers radiality (see below). Anatomical (unbiased T_1-weighted) and mean $b = 0$ vol (from the processed dMRI data) were then co-registered using boundary based registration (Greve and Fischl, 2009), as implemented in FSL (Jenkinson et al., 2012). Using this information, we projected the GM/WM and pial surfaces, as well as the mid-gray matter surface (aligned across subjects for the 7T data), to diffusion space for each individual. The inner and outer gray matter surfaces were used to compute cortical thickness and cortical depth dependent surfaces relative to the local thickness. Specifically, ten surfaces were generated at relative cortical depths, ranging from 0% (GM/WM interface) up to 90% (GM/pia interface), by sampling along the direction given by the surface normal at each vertex. Note that this analysis computes cortical depth levels relative to the local thickness using an equidistant approach, and thus does not respect the preservation of volume of the different cortical layers across sulci and gyri (Waehnert et al., 2014). However, at the resolution of our acquisitions (i.e. 1.05 mm isotropic, and 1.25 mm isotropic) the difference between equivolume and equidistant approaches is negligible (Kemper et al., 2017).

In dMRI space, we computed, for every surface vertex and at every cortical depth, the dot product between each fiber orientation produced by "BedpostX" (up to three, thresholded by their respective volume fraction $f > 5\%$) and the vertex normal. Radiality was estimated, for every vertex and at every cortical depth, as the complementary angle to the inverse cosine of the dot product (i.e. radiality is defined to be 90° for fibers that are locally orthogonal to the surface). The estimated radiality values (up to three values, one per estimated fiber orientation, per vertex and cortical depth) were sorted vertex-wise (within each cortical depth)

[1] https://db.humanconnectome.org.

[2] http://dsi-studio.labsolver.org/.

[3] http://trackvis.org.

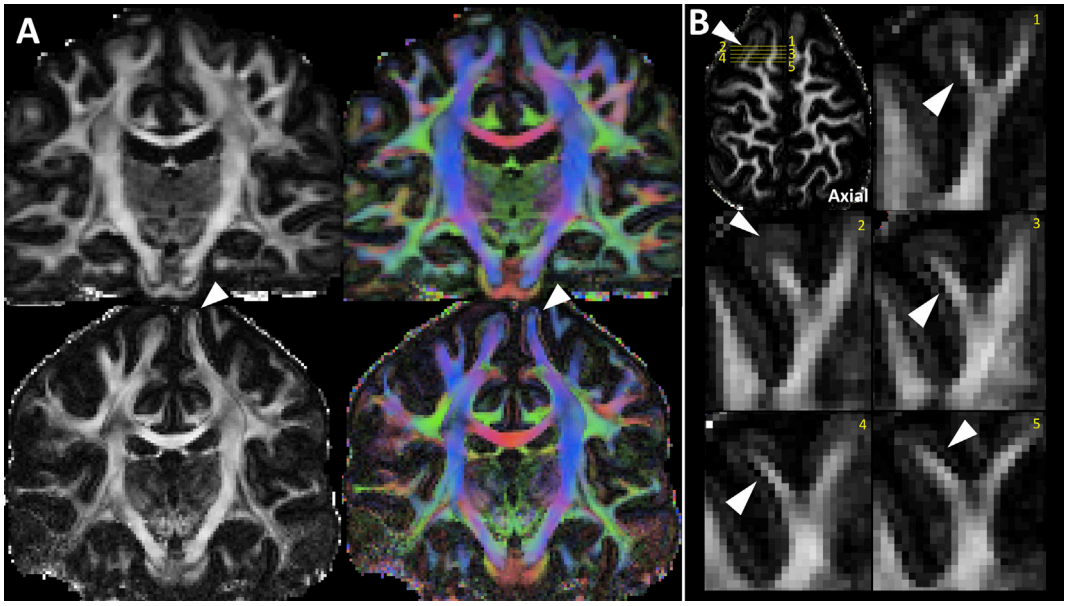

Fig. 3. Panel A: Examples of coronal slices showing fractional anisotropy (FA) and principal direction of diffusion from diffusion tensors, for representative 3T (top) and 7T (bottom) datasets from two different subjects. Color code for principal direction of diffusion is red: left – right, green: anterior – posterior, blue: inferior – superior. Panel B: Depiction of a low FA band in the right superior frontal gyrus showing higher FA in the gyral crown, compared to sulcal wall and fundus.

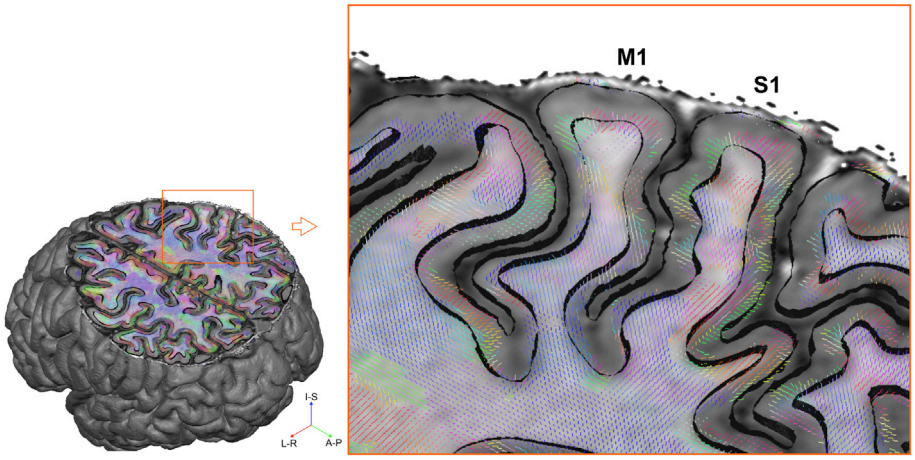

Fig. 4. Volumetric visualization of estimated primary fiber (after thresholding orientations with volume fraction $f > 0.05$), superimposed on the estimated pial and white matter/gray matter boundary from a representative 7T dataset. Color code for primary fibers orientation is red: left – right, green: anterior – posterior, blue: inferior – superior. The few fibers located near the pial surface are spurious orientations associated to noisy dMRI signal outside the brain.

from the most radial (90°) to least radial (0°). For every cortical depth, normalized histograms were obtained by counting the number of vertices within 1-degree bins of radiality values (from 0 to 90°), and dividing each histogram by the maximum count (across cortical depths). Vertices in the medial portion of the surfaces corresponding to the anatomical location of the corpus callosum were excluded. Note that, because of the lower resolution of the dMRI data (compared to anatomical scans), we considered information aggregated in three (non-overlapping) cortical depths relative to local thickness (0–10%, 40–50% and 80–90%). Finally, radiality histograms were also partitioned based on the curvature of the cortical surface. For this, we classified vertices in three categories based on the local curvature: gyral crowns (curvature between −1 and −0.1), sulcal walls (curvature between −0.1 and 0.1), and sulcal fundi (curvature between 0.1 and 1). Note that this partition is based on curvature, as estimated by Brainvoyager, and produced results similar to previous studies (Sotiropoulos et al., 2016), as it can be seen from Fig. 12A (compared to Fig. 8 in (Sotiropoulos et al., 2016)).

Results and discussion

First, we show how high resolution 7T dMRI can be used to characterize the organization of fibers at the GM/WM interface and within the cortex. We present qualitative results describing the orientation of primary fibers, as well as crossing fibers, respectively estimated using the diffusion tensor and multi-shell "ball & stick" model. We also describe the tractography results in the motor cortex (M1 and S1). Consistent with previous studies, e.g. (Anwander et al., 2010; Kleinnijenhuis et al., 2013; McNab et al., 2013) either *ex-vivo* or *in-vivo* with partial brain coverage or limited spatial resolution, we observe both radial and tangential orientations throughout the brain, with variations depending on the cortical depth or areas. Radial fibers appear to dominate, which is in line with developmental studies (McKinstry et al., 2002) supporting that cortical axonal processes and dendrites from pyramidal cells constitute the main source of contrast for cortical dMRI (Kroenke et al., 2007; Kleinnijenhuis et al., 2013).

Beyond these observations, however, we also present results on the organization of crossing fibers at various cortical depths. This had, so far, only been demonstrated *ex-vivo* (Dyrby et al., 2011; Kleinnijenhuis et al., 2013; Leuze et al., 2014; Aggarwal et al., 2015), with complex fiber configurations in the band of Gennari, dominant radial orientations throughout the cortex, and tangential orientation in layers I and VI.

Second, we present a quantitative surface-based analysis of depth-dependent radiality measure, for all significant fiber orientations (up to three). We compare 3T and 7T data, and demonstrate variations of radiality across the cortex, and across cortical depths. Cortex-based aligned surfaces are also used to study the spatial distribution of radiality, for each cortical depth grouped across subjects. We note that, as described in the methods section, even though it is technically possible to subdivide the cortex into up to ten equally spaced depth levels, we elected to only use three relative cortical depths (superficial, middle and deep) for all results presented in this paper. This accounts for the actual resolution of our measurements, which affords at best three voxels at a given cortical location along the surface normal, from white matter to gray matter (considering an average cortical thickness of about 3 mm).

To the best of our knowledge, this is the first report of *whole brain* high resolution HARDI 7T data with high *b*-value, which enables the comprehensive *in-vivo* examination of the cortical microstructure. A previous study (Anwander et al., 2010) reported whole brain 7T dMRI data acquired at 1.5 mm isotropic resolution, and successfully demonstrated varying radiality patterns across the cortex. Another recent study (Sotiropoulos et al., 2016) used, and combined, 3T and 7T HCP dMRI data to successfully reduce the gyral bias of primary fiber orientations at the GM/WM interface. Similarly, another recent study (Fan et al., 2017) introduced a novel method (HIBRID) to combine 3T dMRI data acquired at different spatial resolutions and *b*-values (8000 s/mm^2 at 2 mm isotropic, and 1500 s/mm^2 at 1 mm isotropic), and incorporate priors from T_1-weighted images, to study diffusion properties in the WM and GM. Although it does not focus on fiber orientation (and gyral bias) or crossings, another recent work (Calamante et al., 2017) analyzed the 3T HCP dMRI data using constrained spherical deconvolution to study the average (i.e. not cortical depth dependent) apparent fiber density in the cortex, as a complementary tool to myelin-based MRI techniques.

We confirm overall greater fiber radiality in the primary motor cortex, compared to the somatosensory cortex. We demonstrate that high resolution dMRI data enables the improved reconstruction of radial fibers in sulcal fundi, as well as in the superficial depths of the somatosensory cortex. It also enables the recovery of fiber orientations which gradually transition from the white matter into the cortex, thereby mitigating gyral bias. We illustrate this particular question with tractography results in the primary motor and somatosensory cortices. Finally, we show that high resolution dMRI data permits the identification, to some extent, of tangential fibers in the superficial depths throughout the cortex. This could be explained by a higher contribution to our data of information coming from the plexus of Exner, but could also be ascribed to residual partial volume effects from the cerebrospinal fluid (as also discussed in e.g. (McNab et al., 2013)). Note however that, if partial volume effects were a strong contributor to the results in superficial cortical depths, we would also expect more tangential fiber orientations in the 3T data (due to their lower resolution), which is not the case in our analysis.

It is important to note that our analysis strategy does not account for pulsatile brain motion, which can affect high resolution (diffusion) MRI data. Blurring artifacts, typically introduced by such pulsatile movements, likely affects our 7T data as well as the 3T HCP data (although to a lesser degree due to the lower spatial resolution). Nonetheless, our results show improved agreement with the neuroanatomy for the 7T data, compared to 3T. These results could likely be further improved by utilizing techniques (e.g. specialized pulse sequence) that mitigate pulsatile motion artifacts.

Fiber orientation patterns in the cortex

As reported previously in several studies, the most striking feature of cortical fibers orientation is their radiality, going from GM/WM surface to superficial depths, throughout the cortex, as shown qualitatively in Fig. 5 for three individual subjects. This is particularly visible in the transverse views (Fig. 5A) of the primary motor cortex, as well as the frontal and occipital cortices where green and red fiber orientations respectively denote anterior-posterior and medial-lateral fiber directions. This organization is further illustrated in coronal and sagittal views (Fig. 5B and C), where insets and white arrows (Fig. 5B, C and 5D) highlight the variation of fiber radiality with cortical depth and curvature in M1. Radiality appears to increase from deep to superficial cortical depths. This was previously reported using *in-vivo* and *ex-vivo* data (Kleinnijenhuis et al., 2013, 2015; McNab et al., 2013; Aggarwal et al., 2015), and is quantified (presented next) from our data using cortical depth dependent radiality maps and histograms. We find that this behavior is particularly noticeable in the gyral walls. Reduced radiality in the lower cortical depths is likely due to a combination of two phenomena: 1) fibers inserting at an angle into the cortex (at the GM/WM interface of the gyral walls), and 2) crossing fiber configurations in the deep gray matter. The former is quantified (presented next) using cortical depth dependent radiality maps and histograms. The latter is supported by the band of low FA previously described (Fig. 3), and in agreement with the presence of both radial and tangential fibers in *ex-vivo* dMRI and silver-impregnated sections (Aggarwal et al., 2015) of the infra-granular layers. Dense axonal fibers and apical dendrites were also shown with silver impregnation in the middle layer, which supports the increase in FA and radiality in the middle GM in our data (Figs. 3 and 5).

In sulcal fundi, we find that tangential orientations dominate, especially in the deep and middle gray matter, consistent with the dense transverse fibers inserting into the cortex at sharper angles. We also identify a significant number of locations (yellow arrows in Fig. 5) with radial fiber only in the superficial cortical depth. These findings are consistent with both *ex-vivo* (Leuze et al., 2014), and *in-vivo* (Kleinnijenhuis et al., 2015) data with partial coverage of the brain (hemispheric medial walls). In addition, combining 3T and 7T dMRI data recently revealed slightly increased radiality in histograms estimated in sulcal fundi of the whole cortex (Sotiropoulos et al., 2016).

Fig. 5 also shows specific fiber orientation in the somatosensory cortex, with significantly reduced radiality as shown by fewer anterior-posterior and medial-lateral orientations. Fig. 5C and D (left) show sagittal slices through the pre- and post-central gyri and primarily inferior-superior fiber orientations (blue lines) are seen in S1 gyral crown and wall. We demonstrate next that this is a consistent pattern across subjects and cortical depths. It has also been widely reported *in-vivo* (McNab et al., 2013), and possibly explained by the sparsity and smaller size of radial pyramidal cells in S1 which would preclude dMRI data from capturing intra-cortical radial orientations. Radial orientations in S1 have been reported in an *ex-vivo* study (Aggarwal et al., 2015) in the upper cortical layers, and confirmed by sliver-impregnation which showed significant tangential fibers in infra-granular layers and “fine vertically-oriented fibers” in upper layers (up to III). Our data successfully demonstrates some level of radiality in the middle to superficial depths of S1 gyral walls, as illustrated in Fig. 5C and D (left) by the blue arrows. We partly attribute this to the higher spatial resolution and combination of three *b*-values used to acquire our 7T dMRI data.

Fiber crossings in the deep cortical gray matter

The *q*-space sampling, comparable to the 3T HCP dMRI acquisitions albeit with slightly less directions per shell because of the longer TR at 7T, enables the estimation of crossing fibers at different cortical depths. This had only been shown *ex-vivo* so far, but our results illustrate that high resolution dMRI may be useful in recovering radial and tangential fiber orientations in the deep gray matter.

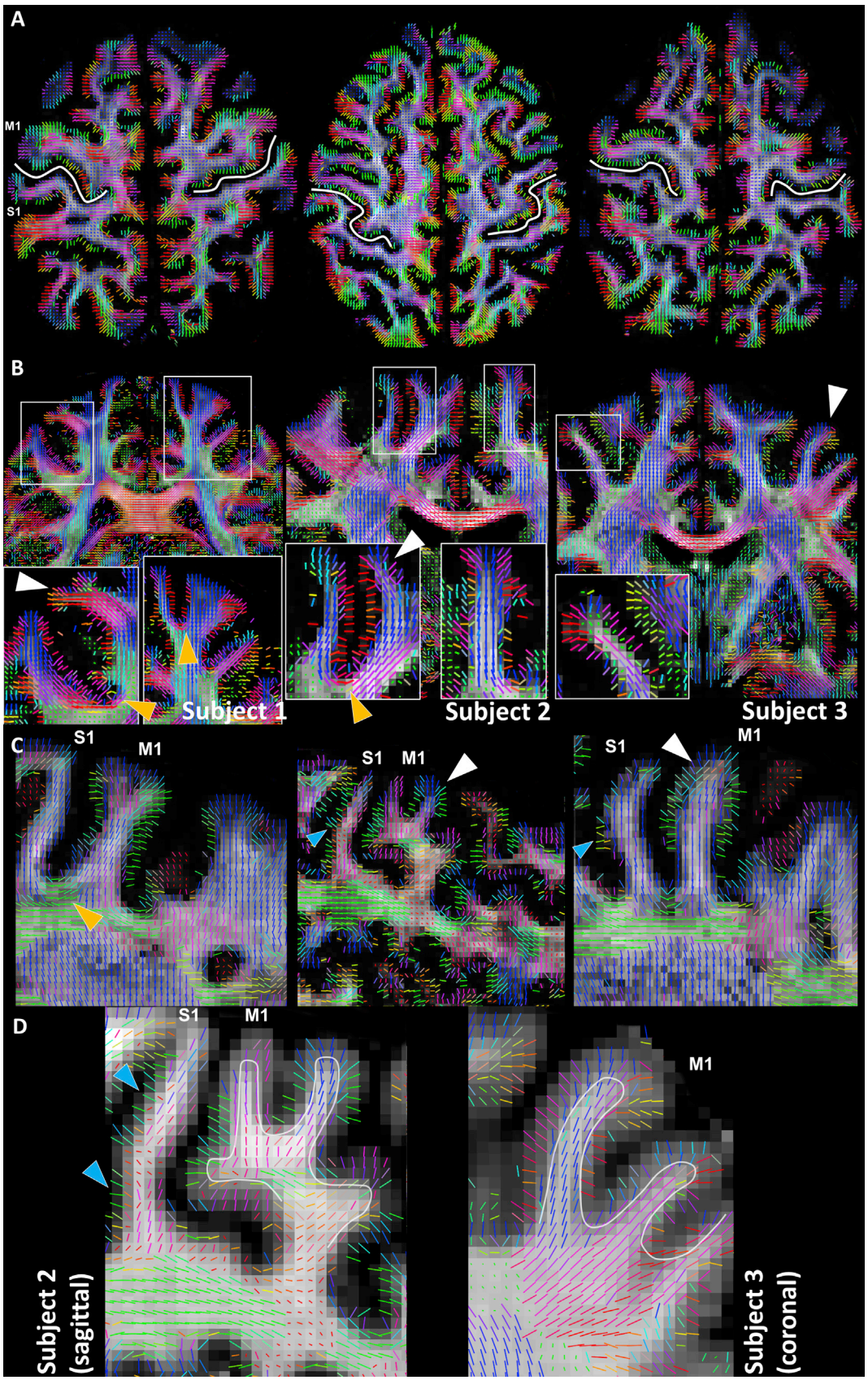

Fig. 5. Primary fiber orientations estimated from 7T HARDI data for three representative subjects (1, 2 and 3), in the primary motor (M1) and somatosensory (S1) cortical areas. Maps are obtained after thresholding orientations with volume fraction $f > 0.05$. Color code for primary fibers orientation is red: left – right, green: anterior – posterior, blue: inferior – superior. Background gray-level images are the total volume fraction of anisotropic compartments obtained from the multi-shell ball & stick model fit. Arrows highlight areas with mostly radial (white) or tangential (yellow) fiber orientations, and some level of radiality in S1 gyral walls (blue). The white lines in Panels A and D were manually defined to represent respectively the central sulcus, and the boundary between gray and white matter.

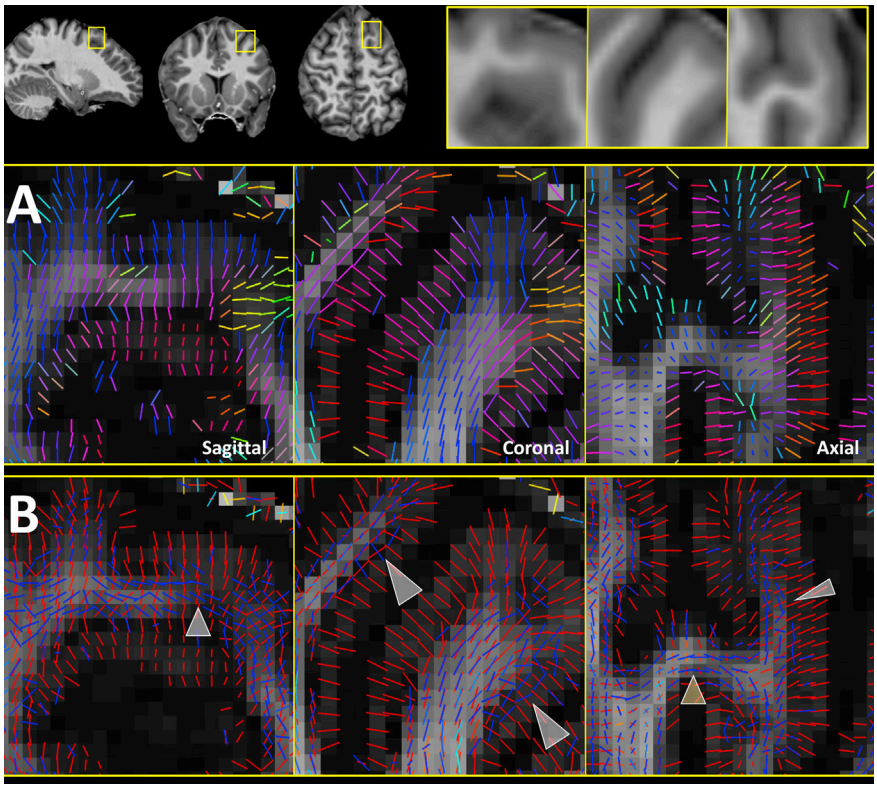

Fig. 6. Panel A: Fiber orientation reconstruction in and around the left middle frontal gyrus; principal direction of diffusion from diffusion tensors. Color code for principal direction of diffusion is red: left – right, green: anterior – posterior, blue: inferior – superior. Panel B: Fiber orientation reconstruction in and around the left middle frontal gyrus; orientations from fiber crossing modeling (ball & stick). 7T data from a representative subject. Arrows highlight areas with crossing fibers configurations. Background gray-level images are the fractional anisotropy (FA).

Fig. 6 shows fiber orientations from the diffusion tensor (6A) and multi-shell ball & stick model (6B) for the same brain area. We chose the middle frontal gyrus (yellow boxes and insets from the high resolution unbiased T_1 images in Fig. 6) as the low FA band tends to be particularly clear in this area, especially in coronal slices. In this view (Fig. 6A), the lateral part of the gyral wall as well as the gyral crown contain fiber orientations (from DTI) which insert into the cortex at an oblique angle. When considering results from the ball & stick model (Fig. 6B), it can be seen that several near 90° crossing fibers configurations are identified in those areas (white arrows). The red orientations represent the primary fibers, defined at each voxel as the compartment with the highest volume fraction in the ball & stick model. These orientations closely match those obtained from DTI. The blue orientations represent the secondary fibers. They follow a spatially consistent pattern and largely correspond to tangential fibers, in agreement with the fact that horizontal fibers in deep gray matter may be less dense and/or smaller. It is important to note, however, that while our data and previous studies (Miller et al., 2011) support that the low FA band lies entirely within the gray matter, the characterization of partial volume effects between white matter and gray matter, and their influence on these results, would be required to understand and mitigate potential contribution to the diffusion signal from the white matter, in other brain areas.

Reduced gyral bias and tractography

Better reconstruction of fibers inserting gradually into the gyral wall, and radial to the superficial cortical depth in the sulcal fundi, should improve tractography results near the cortex by reducing the gyral bias, which we describe next. Fig. 7A shows tractography results in the primary motor cortex (yellow inset), with two different levels of streamlines density to enhance the structure of the estimated fiber bundles. The most prominent and important feature is the ability to capture connections spanning the gyral crown and wall, with streamlines progressively bending into the cortex. Because of gyral bias (Sotiropoulos et al., 2016), streamlines typically aggregate in the most central part of the gyral crown, but this appears to be minimized in Fig. 7A. We do note that, while the gyral bias is reduced, streamlines still appear slightly denser in the gyral crown.

Fig. 7B shows the tractography results at different anterior-posterior locations (upper row) within M1. This is achieved by using each slice as a filter to only show streamlines passing through it. The yellow arrows (middle row) indicate the sulcal fundus where fibers connecting the two gyri can be seen. Significantly improved reconstruction of fiber pathways in both gyri can be noticed. Additionally, we map fractional anisotropy values on streamlines (lower row) to illustrate their variation with cortical depth. Careful inspection reveals bands of low FA in the gyral walls (delineated by white lines in Fig. 7B), as previously discussed and related to crossing radial and tangential fibers. At cortical depths immediately more superficial, increased FA is also noted, followed by a decrease. Although visual inspection of fiber orientations (previous section) did not enable us to identify reduced radiality in the uppermost depths of gyral crowns and walls, likely due to less organized microstructure and/or smaller neurites, this has been previously reported (Kleinnijenhuis et al., 2013; McNab et al., 2013).

Fig. 8A and B presents similar tractography results in a different subject and at different medial-lateral locations (upper row) in M1 and S1. Comparable results are obtained in M1 for streamline orientation (reduced gyral bias) and anisotropy. Additionally, it can be seen in Fig. 8B (middle row, blue arrows) that streamlines follow a path that is mostly straight into the gyral crown with few radial lateral projections into the gyral wall, as described in the previous section. We clarify that streamlines with high FA in the posterior part of S1 originate from more medial WM locations, and not from the posterior gyral wall.

Supplemental video S1 present a three-dimensional view (movie) of the tractography results presented in Fig. 7A and B.

Supplementary video related to this article can be found at https://doi.org/10.1016/j.neuroimage.2018.05.010.

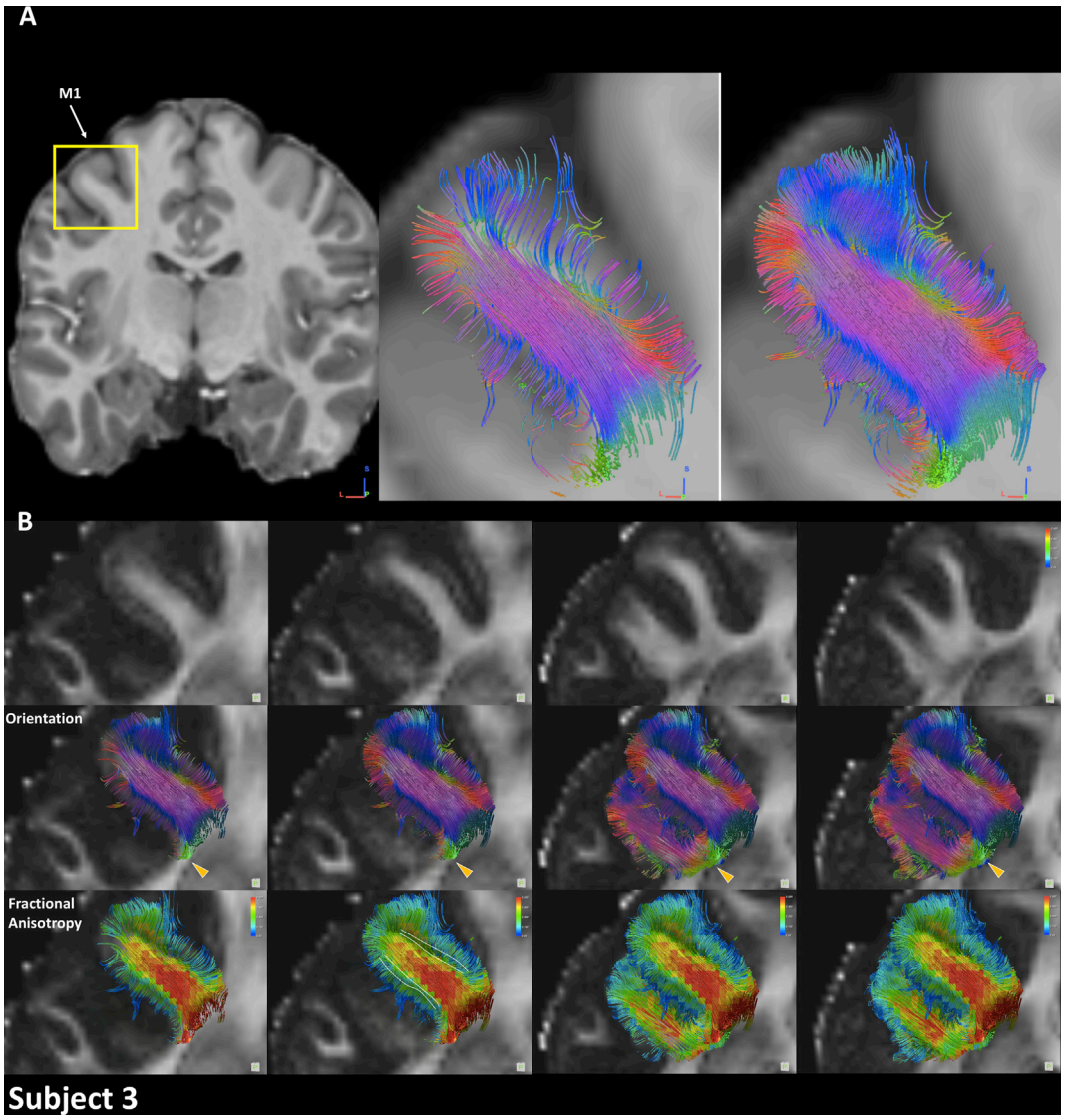

Fig. 7. 7T Tractography (Euler integration using Gaussian radial basis functions for orientation interpolation with 10,000 streamlines) from the primary fiber orientation for representative Subject 3, in the primary motor cortical area. Panel A: 1000 streamlines shown in center image and 5000 streamlines shown in right image. Background image is unbiased T1-weighted data. Panel B: Coronal views in posterior to anterior locations (from left to right columns). Background gray-level image is fractional anisotropy (FA). In the middle row, streamlines color code represents the fiber local orientation (red: left – right, green: anterior – posterior, blue: inferior – superior). In the bottom row, streamlines color code represents FA values.

Surface-based analysis of depth-dependent radiality

Fig. 9 shows representative (two subjects: one for 7T and one for 3T data) radiality maps of the most perpendicular fiber orientation (from the three estimated fiber compartments using the ball & stick model) for deep, middle and superficial cortical depths on inflated surfaces for 3T and 7T data. The most striking feature is the purple/dark blue line located posterior to the central sulcus and corresponding to S1. It is consistent with tangential orientations in the deeper gray matter of S1 gyral wall. 7T maps appear to more consistently find radial orientations in the crowns of the pre- and post-central gyri. In these representative subjects, in addition to S1, parts of the temporal cortex including the lateral Heschl's gyrus and regions within the planum polare bordering the insular cortex, as well as parts of the superior temporal sulcus and superior parietal cortex, exhibit a strong tangential orientation, although they were not as clearly identified at 3T. The secondary somatosensory cortex was also found to have tangential orientation in both 3T and 7T maps. Finally, the frontal and occipital cortices were found to be largely characterized by radial orientation. There are also slightly more green and yellow areas at 7T, putatively corresponding to fibers entering the cortex at oblique angles (vs. 90° at 3T).

In the middle cortical depths, there appears to be a global shift towards more radial orientations throughout the cortex in both 3T and 7T data, consistent with higher anisotropy as previously described. This effect seems stronger at 3T, which may reflect increased gyral bias at 3T. In superficial gray matter, surviving fiber orientations stay mostly radial at 3T but shift, especially in the frontal and temporal areas to less radial orientation at 7T. We hypothesize that this may reflect complex fiber organization (e.g. band of Exner) or simply fewer and/or smaller radial fibers in these areas (Kleinnijenhuis et al., 2015). Interestingly the medial Heschl's gyrus appears consistently as a radial “island” across all depths (Fig. 9).

These results are largely preserved, in the 7T group cortex-based aligned radiality maps, shown in Fig. 10. The entire inferior to superior aspect of S1 is consistently identified as tangential, with fibers becoming progressively more radial towards the pre- and post-central gyral crowns, especially in the middle gray matter. The parietal and temporal cortices show a very consistent pattern of tangential fiber orientations as well, in

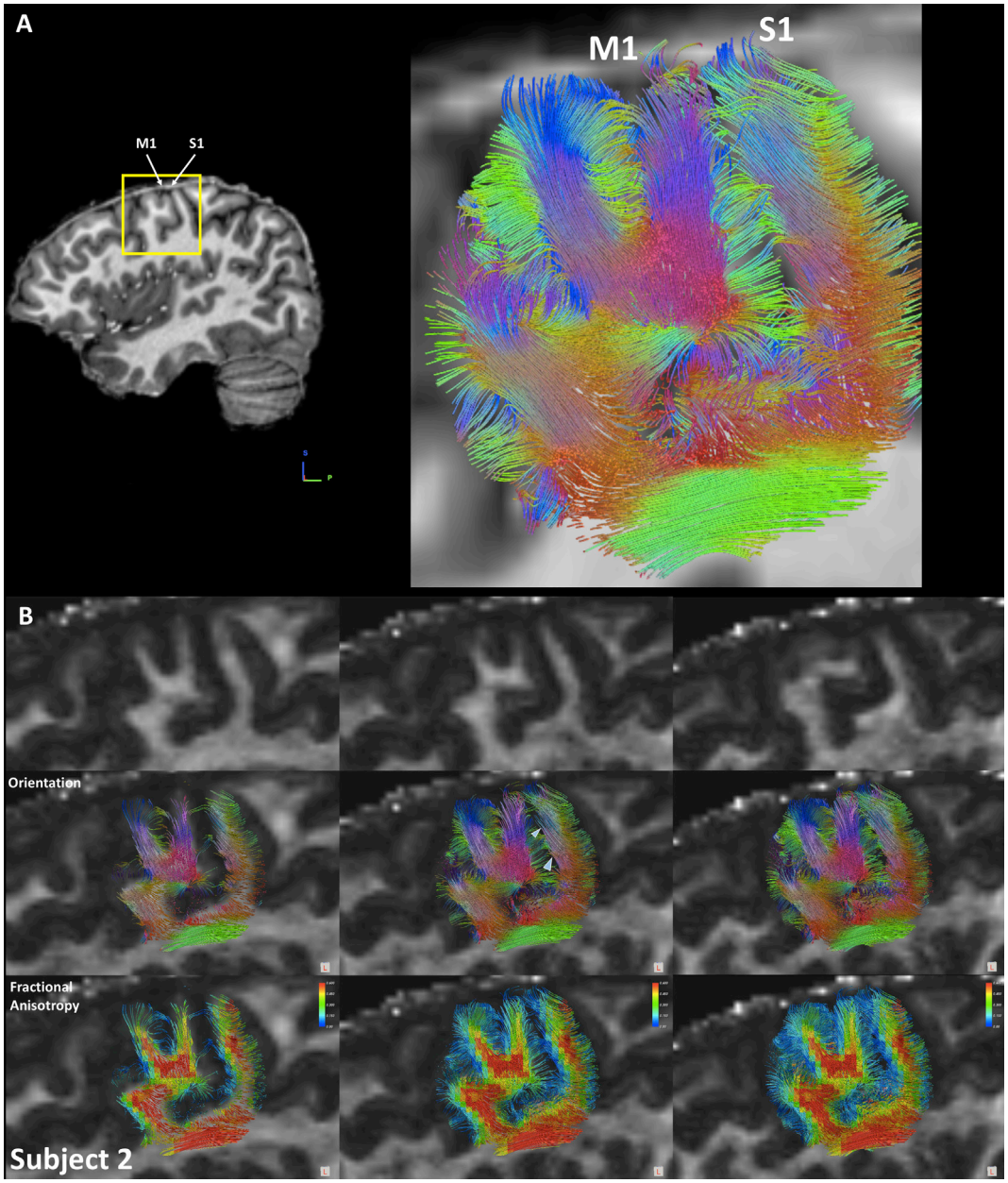

Fig. 8. 7T Tractography (as Fig. 7) for representative Subject 2, in the primary motor and somatosensory cortical areas. Panel A: 5000 streamlines shown in right image. Background image is unbiased T1-weighted data. Panel B: Sagittal views in medial to lateral locations (from left to right columns). Background gray-level image is fractional anisotropy (FA). Color codes are identical to Fig. 7.

particular the planum temporale and planum polare, and the superior bank of the superior temporal sulcus. Note that while the lateral aspect of Heschl's gyrus exhibits mostly tangential orientations (McNab et al., 2013), the most medial portion shows more radial fibers. This characteristic is in agreement with the fiber orientation of primary auditory areas, as identified with myelin stains (see e.g. (Nieuwenhuys, 2013)). Finally, we also note tangential orientations in inferior frontal and pre-frontal areas which were present but not as clear in the individual 7T data in Fig. 9. The shift toward more radial orientations in the middle gray matter can also be seen in the group map, especially in the superior frontal and pre-frontal areas, insular, inferior parietal and occipital cortices. These findings are mostly preserved in the superficial depth, with a slight shift toward lower radiality. We also note that a large portion of the voxels within the superficial depth contains primary fiber orientations, even after thresholding with volume fraction $f > 0.05$, which was done for all experiments.

Compared to 3T however, 7T dMRI data detected slightly less cortical voxels with one, two or three fibers (see statistics in Table 1). This is partly explained by the fact that 7T data had about 25% fewer gradient directions than the 3T data, and reduced q-space angular sampling typically results in increased uncertainty for fiber orientation estimation. Despite having lower proportions of cortical voxels where the data supports fibers (mostly secondary and tertiary fibers), we emphasize that the actual orientation of those detected fibers, described in this paper, still provide improved characterization of cortical radiality and reduce the gyral bias. This will be also supported by the depth-dependent histograms presented below.

Depth-dependent radiality histograms

In Fig. 11, we present histograms of radiality values (with respect to the cortical surfaces) for all fiber orientations and all cortical areas.

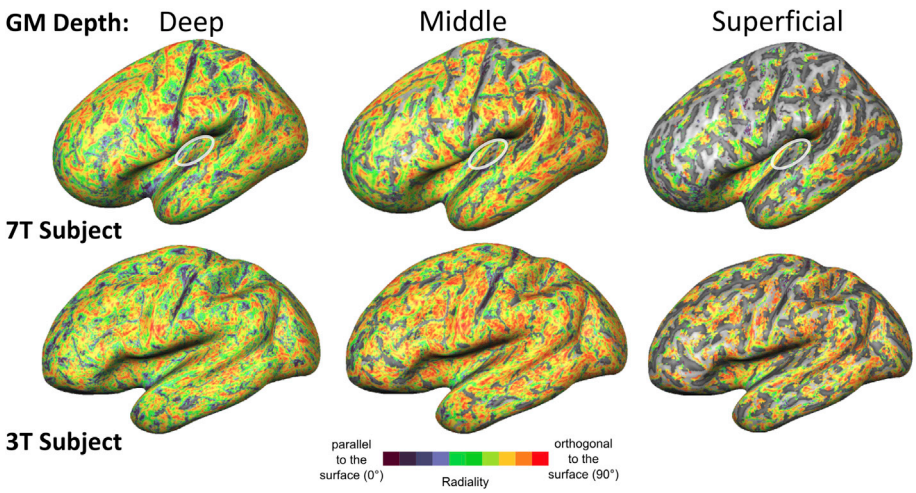

Fig. 9. Cortical-depth dependent radiality maps of the most perpendicular fiber orientation, in representative subjects for 3T and 7T (Maps obtained after thresholding orientations with volume fraction $f > 0.05$). Deep, middle and superficial maps represent information aggregated from three (non-overlapping) cortical depths relative to the local thickness (0–10%, 40–50% and 80–90%).

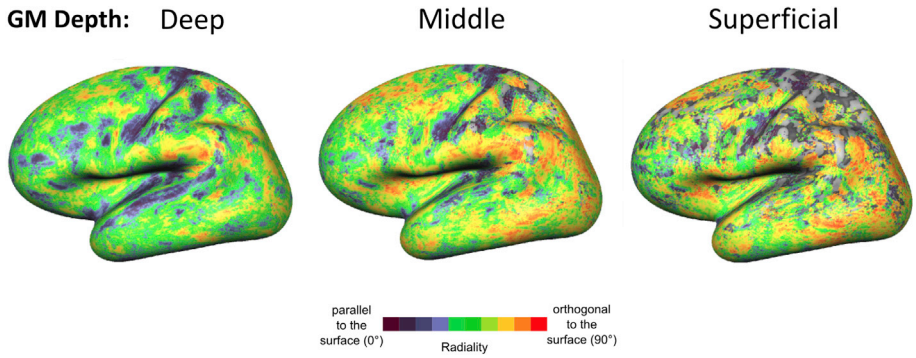

Fig. 10. Group cortical-depth dependent radiality maps of the most perpendicular fiber orientation, after cortex-based alignment of 7T datasets (N = 6). (Maps obtained after thresholding orientations with volume fraction $f > 0.05$). Deep, middle and superficial maps represent information aggregated from three (non-overlapping) cortical depths relative to the local thickness (0–10%, 40–50% and 80–90%).

Table 1
Proportion of cortical voxels (including all depths) with primary, secondary and tertiary fibers, using 3T and 7T data and detected with the ball & stick model (with volume fractions $f > 0.05$).

Proportions	Primary fiber	Secondary fiber	Tertiary fiber
3T	65 ± 3%	27 ± 2%	4 ± 0.5%
7T	59 ± 3%	11 ± 3%	1 ± 0.2%

Orientations were sorted, at each voxel, not by their volume fraction, but rather by their radiality (from most radial to most tangential with respect to the surface). Usually, orientations with the largest weight correspond to the most radial fibers, but secondary orientations can sometimes also represent those most radial fibers as there is no constraint in the ball & stick model for orientation with respect to surfaces. Sorting fibers by radiality therefore makes interpretation of our results easier with respect to neuroanatomy.

First, radiality of primary fibers follow a similar pattern in the deep gray matter at 3T and 7T. Primary fibers span a range of angles between 0 and 80–85°, with 7T data supporting slightly more orientations below 15°. This may reflect fibers entering the cortex at smoothly varying angles. Secondary and tertiary fibers in deep gray matter at 3T and 7T are oriented in a similar fashion, with low angles below 20°. This is likely related to crossing horizontal fibers in the band of low FA, as described earlier and illustrated in Fig. 6. Next, in middle gray matter, fibers become significantly more radial for both 3T and 7T datasets, although secondary orientations are also detected with angles between 0 and 60°. Increased radiality in middle gray matter was shown previously *in-vivo* (McNab et al., 2013; Kleinnijenhuis et al., 2015) with angles around 50–60°. This is mostly consistent with our findings, although we found angles in the 60–90° range, possibly because the ball & stick model better captures crossing fiber configurations. There is no previous whole brain *in-vivo* work demonstrating crossing fibers in the middle cortical depths, to the best of our knowledge, but this has been shown *ex-vivo* in the bands of Baillarger (Dyrby et al., 2011; Leuze et al., 2014; Aggarwal et al., 2015). The main difference between 7T and 3T datasets, in the middle gray matter, is that 7T data shows a wider distribution of primary fiber orientations, in the range between 60 and 90° with a mean around 75°, while 3T data is more skewed and concentrated around 90° orientations. Although such differences may be due to increased gyral bias at 3T, other factors such as crossing fibers configurations and inter-subjects variability should not be discarded and may also contribute to this effect. This could be matter for further investigations, possibly using optimized acquisition parameters in conjunction with high spatial resolution. Finally, a difference can be noticed between 3T and 7T in superficial gray matter, where the primary fibers span a range of angles between 0 and 80–85° at 7T, while they are concentrated around 80° (mostly radial) at 3T. 7T results are more in line with both *in-vivo* and *ex-vivo* data possibly relating to radial and tangential orientations in layer I/II. Secondary crossing (tangential) fibers are detected at 3T around 10°, as well as at 7T with angles between 0 and 30°. This therefore suggests that the higher spatial resolution 7T dMRI might enable improved estimation of tangential fibers in superficial gray matter.

We conclude with results shown in Fig. 12 for cortical depth

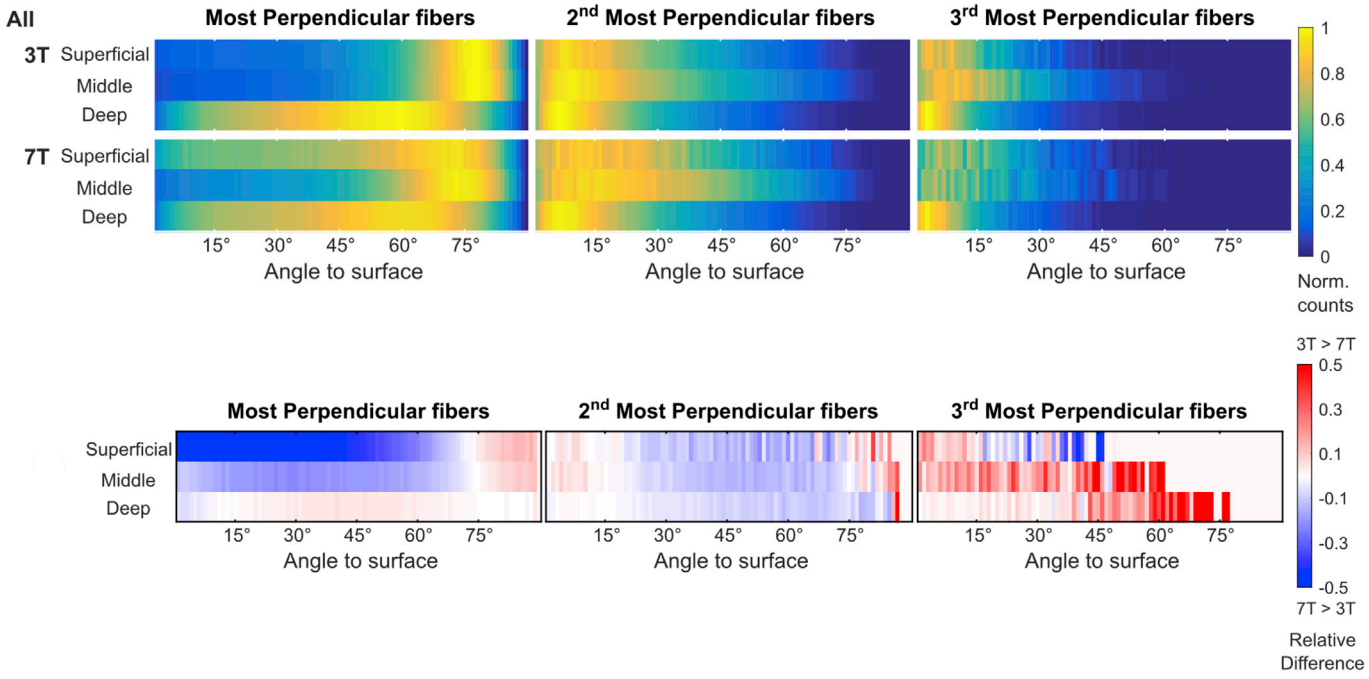

Fig. 11. Group cortical-depth dependent histograms of angles (with respect to the cortical surface) for each fiber orientation, for 3T and 7T data. Deep, middle and superficial histograms represent information aggregated from three (non-overlapping) cortical depths relative to the local thickness (0–10%, 40–50% and 80–90%). Fiber orientations are sorted (most, second most and third most perpendicular), at each voxel, by their radiality (from most radial to most tangential with respect to the surface).

dependent radiality histograms in the gyral crowns, walls, and sulcal fundi, as initially discussed in section 3.3. In sulcal fundi, fibers in deep gray matter are mostly tangential (see sections 3.1 and 3.3), but also exhibit more radiality (60–75°) in the 7T data, which is a possible source of reduced gyral bias. Although fibers are mostly radial at 3T, in the middle and superficial gray matter (60° and above), they appear to span a broader range of angles in the 7T data (0–80–85°), with greater radiality in the middle cortical depth. This may reflect an increase in radiality contrast, thereby allowing one to better capture complex fiber orientation patterns in sulcal fundi (i.e. not only tangential). Similar trends across depths are observed in the gyral crowns and walls, albeit with even greater radiality in the middle and superficial gray matter, especially at 3T. In that case (3T), most fibers are oriented around 80–85° in middle and superficial gray matter, while they span a range of tangential to more radial orientations in the deep gray matter. The 7T data demonstrate a more gradual transition across cortical depths from tangential to radial (and back to partly tangential) in gyral crowns and walls. We hypothesize that this also contributes to reducing the gyral bias.

We would like to note that the cortical depth dependent radiality characteristics of fiber orientations obtained from the 7T data does not change significantly (despite a small increase in orientations uncertainty), when discarding the $b = 3000\,\mathrm{s/mm^2}$ shell (i.e. similar to the original 7T HCP protocol), or removing an equivalent number of diffusion directions across all three shells. While this seems to indicate that the primary strength of our 7T data, to resolve characteristics of cortical diffusion, comes from its high spatial resolution, more investigations will be required to identify the optimal combination of high *b*-values and high spatial resolution in a single acquisition to resolve gray matter axonal orientation characteristics.

Conclusions

To investigate the organization of axonal trajectories within the cortex at different cortical depths requires high spatial resolution data to reduce partial volume effects and dedicated processing pipelines to fully leverage the information available in such data. Here, we present unique whole brain 7T dMRI data, demonstrating the possibility of studying fiber orientations across cortical depths *in-vivo*. The increased resolution enables a reduction of the gyral bias (i.e. the delineation of gradual fiber insertions into the gyral walls) and detection of architectural features confirmed in *ex-vivo* studies, such as tangential fibers in superficial gray matter, and crossing fibers in middle and deep gray matter. This is the first whole brain cortical depth dependent analysis of *in-vivo* 7T high angular resolution dMRI data, combined with the estimation of crossing cortical fibers. We have also shown the possibility to perform deterministic tractography within the cortex, an effort that is rendered more meaningful by the reduced gyral bias.

Estimating structural connections to/from the gyral walls and sulcal fundi is crucial for building accurate representations of the connectome (Van Essen et al., 2014; Sotiropoulos et al., 2016). Such efforts can be improved by reducing the gyral bias with higher resolution data acquired at 7T (despite lower *q*-space sampling density), as presented in this paper. Together with more advanced tractography methods, the more accurate delineation of cortical insertions in the gyral walls should ultimately prevent streamlines from accumulating in gyral crowns, which is not supported by histological data (Van Essen et al., 1986, 2014).

The cortical depth dependent analysis used in our work must be carefully considered when interpreting the results, see also discussion in (McNab et al., 2013). The cortex thickness is about 3 mm and therefore, in the best-case scenario, each of our cortical depths (deep, middle, superficial) corresponds to about one voxel. While we sampled the fiber orientations and radiality maps along 10 equally spaced surfaces within the cortical ribbon, we report the results in three distinct intervals of cortical depth (0–10%, 40–50% and 80–90%) to minimize partial volume effects. Each of the three intervals should be considered as a mixture of cortical lamina (e.g. V/VI, III/IV and I/II) and interpreted accordingly. Nevertheless, our results show that it is crucial to consider this laminar structure, when analyzing high resolution dMRI data in the cortex, as important features can be highlighted. Our findings and those of previous studies are well supported by *ex-vivo* and histological data.

Additionally, the origin and interpretation of the diffusion signal in the cortex should be carefully addressed, as it is quite different from the

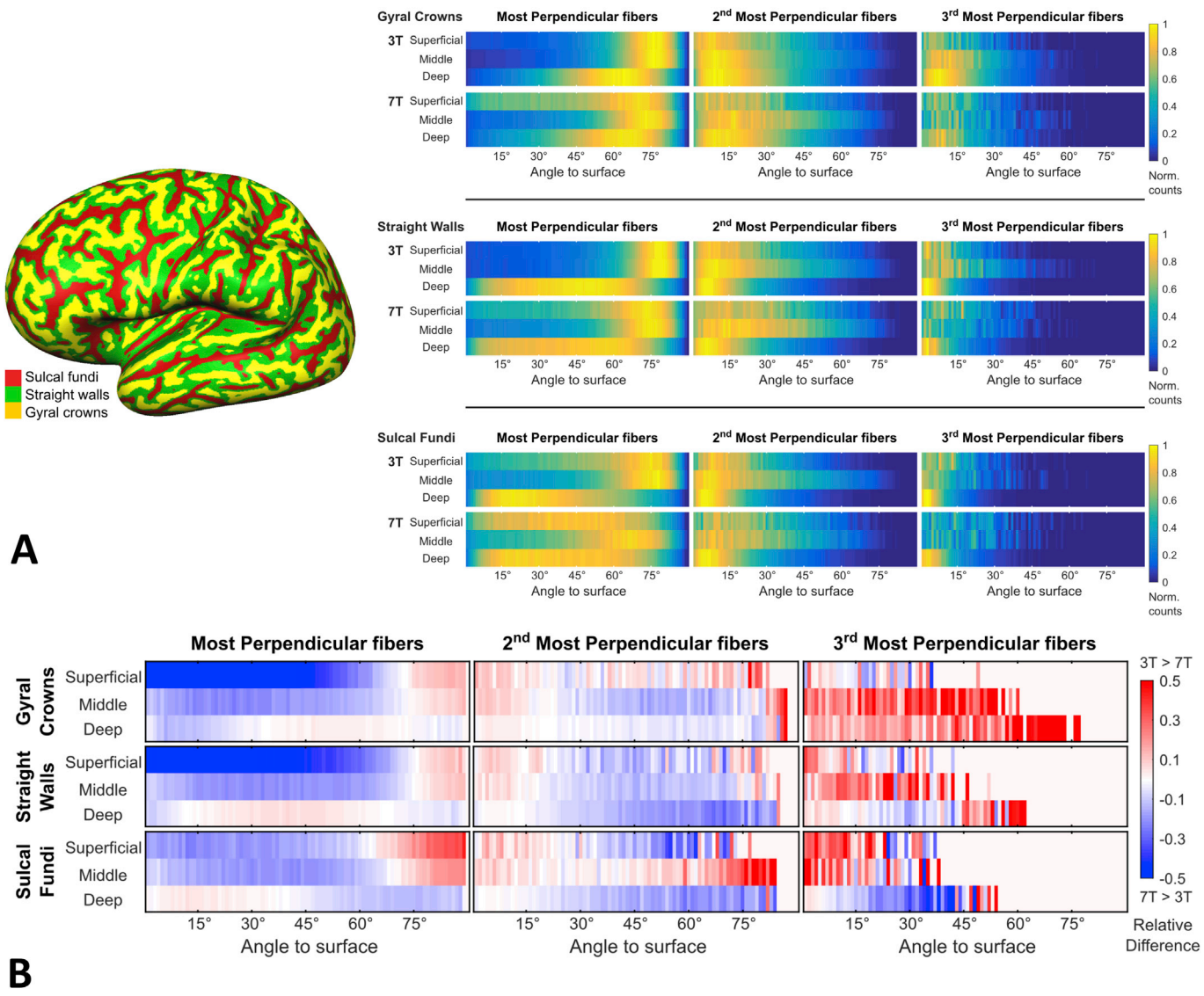

Fig. 12. Panel A: Group cortical-depth dependent histograms, in gyral crowns, walls and sulci, of angles (with respect to the cortical surface) for each fiber orientation, for 3T and 7T data. Panel B: Comparison of 3T and 7T group cortical-depth dependent histograms, in gyral crowns, walls and sulci, of angles (with respect to the cortical surface) for each fiber orientation. Deep, middle and superficial histograms represent information aggregated from three (non-overlapping) cortical depths relative to the local thickness (0–10%, 40–50% and 80–90%). Fiber orientations are sorted (most, second most and third most perpendicular), at each voxel, by their radiality (from most radial to most tangential with respect to the surface).

white matter (Kleinnijenhuis et al., 2013) and likely requires different acquisition parameters and modeling techniques. The cortex is indeed much more heterogeneous than the white matter, with a greater proportion of neuronal cell bodies and glia. In certain cortical areas, axonal processes and dendrites from large pyramidal cells – not only myelinated axonal bundles – constitute some of the primary sources of anisotropy. Diffusion acquisition parameters should therefore be adapted to reflect the smaller size of neurites from which anisotropy arises. In particular, the effective diffusion time (used in, e.g., a pulsed gradient spin echo sequence) should probably be shorter (currently in the 30–40 ms range). Here, we did not investigate the effects or benefits of such protocol optimization. Our main objective was the comparison between the 3T HCP protocol and a time-matched 7T protocol at higher spatial resolution. We would expect that any optimization, for the GM, of diffusion acquisition parameters and analysis would further improve agreement with the neuroanatomy, especially at high spatial resolution, which we show here to have a considerable impact.

Cortical depth dependent analysis of cortical microstructural data may represent an additional and important source of information for the parcellation of cortical areas (e.g. primary sensory areas), the understanding of brain development, aging, and of neurodegenerative processes involved in diseases like Alzheimer's disease or multiple sclerosis. It is therefore crucial to continue and accelerate technical developments in hardware, pulse sequences and computational modeling, so that data with even greater level of details could ultimately be generated on clinical scanners and in shorter acquisition times (Setsompop et al., 2017).

Acknowledgments

This work was supported in part by NIH grants P41 EB015894, P30 NS076408 and U01 EB025144. F.D.M. and O.F.G. were supported by NWO VIDI grant 864-13-012. Data were provided in part by the Human Connectome Project, WU-Minn Consortium (Principal Investigators: David Van Essen and Kamil Ugurbil; 1U54MH091657) funded by the 16 NIH Institutes and Centers that support the NIH Blueprint for Neuroscience Research; and by the McDonnell Center for Systems Neuroscience at Washington University.

Appendix A. Supplementary data

Supplementary data related to this article can be found at https://doi.org/10.1016/j.neuroimage.2018.05.010.

References

Aggarwal, M., Nauen, D.W., Troncoso, J.C., Mori, S., 2015. Probing region-specific microstructure of human cortical areas using high angular and spatial resolution diffusion MRI. Neuroimage 105, 198–207.

Alexander, D.C., Hubbard, P.L., Hall, M.G., Moore, E.A., Ptito, M., Parker, G.J., Dyrby, T.B., 2010. Orientationally invariant indices of axon diameter and density from diffusion MRI. Neuroimage 52, 1374–1389.

Andersson, J.L., Sotiropoulos, S.N., 2015. Non-parametric representation and prediction of single- and multi-shell diffusion-weighted MRI data using Gaussian processes. Neuroimage 122, 166–176.

Andersson, J.L.R., Sotiropoulos, S.N., 2016. An integrated approach to correction for off-resonance effects and subject movement in diffusion MR imaging. Neuroimage 125, 1063–1078.

Andersson, J.L., Skare, S., Ashburner, J., 2003. How to correct susceptibility distortions in spin-echo echo-planar images: application to diffusion tensor imaging. Neuroimage 20, 870–888.

Anwander, A., Pampel, A., Knosche, T.R., 2010. In vivo measurement of cortical anisotropy by diffusion-weighted imaging correlates with cortex type. Proc. Int. Soc. Magn. Reson. Med. 109.

Assaf, Y., Basser, P.J., 2005. Composite hindered and restricted model of diffusion (CHARMED) MR imaging of the human brain. Neuroimage 27, 48–58.

Baillarger, J.G.F., 1840. Recherches sur la structure de la couche corticale des circonvolutions du cerveau. J.-B. Baillière, Paris.

Barazany, D., Assaf, Y., 2012. Visualization of cortical lamination patterns with magnetic resonance imaging. Cereb. Cortex 22, 2016–2023.

Basser, P.J., Mattiello, J., LeBihan, D., 1994. Estimation of the effective self-diffusion tensor from the NMR spin echo. J. Magn. Reson B 103, 247–254.

Bastiani, M., Oros-Peusquens, A.M., Seehaus, A., Brenner, D., Mollenhoff, K., Celik, A., Felder, J., Bratzke, H., Shah, N.J., Galuske, R., Goebel, R., Roebroeck, A., 2016. Automatic segmentation of human cortical layer-complexes and architectural areas using ex vivo diffusion MRI and its validation. Front. Neurosci. 10, 487.

Beaulieu, C., 2002. The basis of anisotropic water diffusion in the nervous system - a technical review. NMR Biomed. 15, 435–455.

Behrens, T.E., Berg, H.J., Jbabdi, S., Rushworth, M.F., Woolrich, M.W., 2007. Probabilistic diffusion tractography with multiple fibre orientations: what can we gain? Neuroimage 34, 144–155.

Braak, H., Braak, E., 1976. The pyramidal cells of Betz within the cingulate and precentral gigantopyramidal field in the human brain. A Golgi and pigmentarchitectonic study. Cell Tissue Res. 172, 103–119.

Calamante, F., Jeurissen, B., Smith, R.E., Tournier, J.D., Connelly, A., 2017. The role of whole-brain diffusion MRI as a tool for studying human in vivo cortical segregation based on a measure of neurite density. Magn. Reson Med.

Chen, H., Zhang, T., Guo, L., Li, K., Yu, X., Li, L., Hu, X., Han, J., Hu, X., Liu, T., 2013. Coevolution of gyral folding and structural connection patterns in primate brains. Cereb. Cortex 23, 1208–1217.

D'Arceuil, H.E., Westmoreland, S., de Crespigny, A.J., 2007. An approach to high resolution diffusion tensor imaging in fixed primate brain. Neuroimage 35, 553–565.

Deistung, A., Schafer, A., Schweser, F., Biedermann, U., Turner, R., Reichenbach, J.R., 2013. Toward in vivo histology: a comparison of quantitative susceptibility mapping (QSM) with magnitude-, phase-, and R2*-imaging at ultra-high magnetic field strength. Neuroimage 65, 299–314.

Dell'Acqua, F., Bodi, I., Slater, D., Catani, M., Modo, M., 2013. MR diffusion histology and micro-tractography reveal mesoscale features of the human cerebellum. Cerebellum 12, 923–931.

Dick, F., Tierney, A.T., Lutti, A., Josephs, O., Sereno, M.I., Weiskopf, N., 2012. In vivo functional and myeloarchitectonic mapping of human primary auditory areas. J. Neurosci. 32, 16095–16105.

Dinse, J., Hartwich, N., Waehnert, M.D., Tardif, C.L., Schafer, A., Geyer, S., Preim, B., Turner, R., Bazin, P.L., 2015. A cytoarchitecture-driven myelin model reveals area-specific signatures in human primary and secondary areas using ultra-high resolution in-vivo brain MRI. Neuroimage 114, 71–87.

Dyrby, T.B., Baare, W.F., Alexander, D.C., Jelsing, J., Garde, E., Sogaard, L.V., 2011. An ex vivo imaging pipeline for producing high-quality and high-resolution diffusion-weighted imaging datasets. Hum. Brain Mapp. 32, 544–563.

Eickhoff, S., Walters, N.B., Schleicher, A., Kril, J., Egan, G.F., Zilles, K., Watson, J.D., Amunts, K., 2005. High-resolution MRI reflects myeloarchitecture and cytoarchitecture of human cerebral cortex. Hum. Brain Mapp. 24, 206–215.

Van Essen, D.C., Newsome, W.T., Maunsell, J.H., Bixby, J.L., 1986. The projections from striate cortex (V1) to areas V2 and V3 in the macaque monkey: asymmetries, areal boundaries, and patchy connections. J. Comp. Neurol. 244, 451–480.

Van Essen, D.C., Ugurbil, K., Auerbach, E., Barch, D., Behrens, T.E., Bucholz, R., Chang, A., Chen, L., Corbetta, M., Curtiss, S.W., Della Penna, S., Feinberg, D., Glasser, M.F., Harel, N., Heath, A.C., Larson-Prior, L., Marcus, D., Michalareas, G., Moeller, S., Oostenveld, R., Petersen, S.E., Prior, F., Schlaggar, B.L., Smith, S.M., Snyder, A.Z., Xu, J., Yacoub, E., Consortium, W.U.-M.H., 2012. The Human Connectome Project: a data acquisition perspective. Neuroimage 62, 2222–2231.

Van Essen, D.C., Smith, S.M., Barch, D.M., Behrens, T.E., Yacoub, E., Ugurbil, K., Consortium, W.U.-M.H., 2013. The WU-minn human connectome Project: an overview. Neuroimage 80, 62–79.

Van Essen, D.C., Jbabdi, S., Sotiropoulos, S.N., Chen, C., Dikranian, K., Coalson, T., Harwell, J., Behrens, T.E.J., Glasser, M.F., 2014. Mapping Connections in Humans and Non-human Primates Aspirations and Challenges for Diffusion Imaging. Diffusion MRI, second ed. Academic Press, San Diego, pp. 337–358.

Fan, Q., Nummenmaa, A., Polimeni, J.R., Witzel, T., Huang, S.Y., Wedeen, V.J., Rosen, B.R., Wald, L.L., 2017. HIgh b-value and high Resolution Integrated Diffusion (HIBRID) imaging. Neuroimage 150, 162–176.

Farooq, H., Xu, J., Nam, J.W., Keefe, D.F., Yacoub, E., Georgiou, T., Lenglet, C., 2016. Microstructure imaging of crossing (MIX) white matter fibers from diffusion MRI. Sci. Rep. 6, 38927.

Geyer, S., Weiss, M., Reimann, K., Lohmann, G., Turner, R., 2011. Microstructural parcellation of the human cerebral cortex - from Brodmann's post-mortem map to in vivo mapping with high-field magnetic resonance imaging. Front. Hum. Neurosci. 5, 19.

Glasser, M.F., Sotiropoulos, S.N., Wilson, J.A., Coalson, T.S., Fischl, B., Andersson, J.L., Xu, J., Jbabdi, S., Webster, M., Polimeni, J.R., Van Essen, D.C., Jenkinson, M., Consortium, W.U.-M.H., 2013. The minimal preprocessing pipelines for the Human Connectome Project. Neuroimage 80, 105–124.

Glasser, M.F., Coalson, T.S., Robinson, E.C., Hacker, C.D., Harwell, J., Yacoub, E., Ugurbil, K., Andersson, J., Beckmann, C.F., Jenkinson, M., Smith, S.M., Van Essen, D.C., 2016. A multi-modal parcellation of human cerebral cortex. Nature 536, 171–178.

Goebel, R., Esposito, F., Formisano, E., 2006. Analysis of functional image analysis contest (FIAC) data with brainvoyager QX: from single-subject to cortically aligned group general linear model analysis and self-organizing group independent component analysis. Hum. Brain Mapp. 27, 392–401.

Greve, D.N., Fischl, B., 2009. Accurate and robust brain image alignment using boundary-based registration. Neuroimage 48, 63–72.

Heidemann, R.M., Porter, D.A., Anwander, A., Feiweier, T., Heberlein, K., Knosche, T.R., Turner, R., 2010. Diffusion imaging in humans at 7T using readout-segmented EPI and GRAPPA. Magn. Reson Med. 64, 9–14.

Helbling, S., Teki, S., Callaghan, M.F., Sedley, W., Mohammadi, S., Griffiths, T.D., Weiskopf, N., Barnes, G.R., 2015. Structure predicts function: combining non-invasive electrophysiology with in-vivo histology. Neuroimage 108, 377–385.

Jaermann, T., De Zanche, N., Staempfli, P., Pruessmann, K.P., Valavanis, A., Boesiger, P., Kollias, S.S., 2008. Preliminary experience with visualization of intracortical fibers by focused high-resolution diffusion tensor imaging. AJNR Am. J. Neuroradiol. 29, 146–150.

Jbabdi, S., Sotiropoulos, S.N., Savio, A.M., Grana, M., Behrens, T.E., 2012. Model-based analysis of multishell diffusion MR data for tractography: how to get over fitting problems. Magn. Reson Med. 68, 1846–1855.

Jenkinson, M., Beckmann, C.F., Behrens, T.E., Woolrich, M.W., Smith, S.M., 2012. Fsl. Neuroimage 62, 782–790.

Kang, X., Herron, T.J., Turken, A.U., Woods, D.L., 2012. Diffusion properties of cortical and pericortical tissue: regional variations, reliability and methodological issues. Magn. Reson Imaging 30, 1111–1122.

Kemper, V.G., De Martino, F., Emmerling, T.C., Yacoub, E., Goebel, R., 2017. High resolution data analysis strategies for mesoscale human functional MRI at 7 and 9.4T. Neuroimage.

Kleinnijenhuis, M., Zerbi, V., Kusters, B., Slump, C.H., Barth, M., van Cappellen van Walsum, A.M., 2013. Layer-specific diffusion weighted imaging in human primary visual cortex in vitro. Cortex 49, 2569–2582.

Kleinnijenhuis, M., van Mourik, T., Norris, D.G., Ruiter, D.J., van Cappellen van Walsum, A.M., Barth, M., 2015. Diffusion tensor characteristics of gyrencephaly using high resolution diffusion MRI in vivo at 7T. Neuroimage 109, 378–387.

Kroenke, C.D., Van Essen, D.C., Inder, T.E., Rees, S., Bretthorst, G.L., Neil, J.J., 2007. Microstructural changes of the baboon cerebral cortex during gestational development reflected in magnetic resonance imaging diffusion anisotropy. J. Neurosci. 27, 12506–12515.

Lenglet, C., Campbell, J.S., Descoteaux, M., Haro, G., Savadjiev, P., Wassermann, D., Anwander, A., Deriche, R., Pike, G.B., Sapiro, G., Siddiqi, K., Thompson, P.M., 2009. Mathematical methods for diffusion MRI processing. Neuroimage 45, S111–S122.

Leuze, C.W., Anwander, A., Bazin, P.L., Dhital, B., Stuber, C., Reimann, K., Geyer, S., Turner, R., 2014. Layer-specific intracortical connectivity revealed with diffusion MRI. Cereb. Cortex 24, 328–339.

Lutti, A., Dick, F., Sereno, M.I., Weiskopf, N., 2014. Using high-resolution quantitative mapping of R1 as an index of cortical myelination. Neuroimage 93 (Pt 2), 176–188.

Markov, N.T., Misery, P., Falchier, A., Lamy, C., Vezoli, J., Quilodran, R., Gariel, M.A., Giroud, P., Ercsey-Ravasz, M., Pilaz, L.J., Huissoud, C., Barone, P., Dehay, C., Toroczkai, Z., Van Essen, D.C., Kennedy, H., Knoblauch, K., 2011. Weight consistency specifies regularities of macaque cortical networks. Cereb. Cortex 21, 1254–1272.

Markov, N.T., Ercsey-Ravasz, M.M., Ribeiro Gomes, A.R., Lamy, C., Magrou, L., Vezoli, J., Misery, P., Falchier, A., Quilodran, R., Gariel, M.A., Sallet, J., Gamanut, R., Huissoud, C., Clavagnier, S., Giroud, P., Sappey-Marinier, D., Barone, P., Dehay, C., Toroczkai, Z., Knoblauch, K., Van Essen, D.C., Kennedy, H., 2014. A weighted and directed interareal connectivity matrix for macaque cerebral cortex. Cereb. Cortex 24, 17–36.

De Martino, F., Moerel, M., Xu, J., van de Moortele, P.F., Ugurbil, K., Goebel, R., Yacoub, E., Formisano, E., 2015. High-resolution mapping of myeloarchitecture in vivo: localization of auditory areas in the human brain. Cereb. Cortex 25, 3394–3405.

McKinstry, R.C., Mathur, A., Miller, J.H., Ozcan, A., Snyder, A.Z., Schefft, G.L., Almli, C.R., Shiran, S.I., Conturo, T.E., Neil, J.J., 2002. Radial organization of

developing preterm human cerebral cortex revealed by non-invasive water diffusion anisotropy MRI. Cereb. Cortex 12, 1237–1243.
McNab, J.A., Jbabdi, S., Deoni, S.C., Douaud, G., Behrens, T.E., Miller, K.L., 2009. High resolution diffusion-weighted imaging in fixed human brain using diffusion-weighted steady state free precession. Neuroimage 46, 775–785.
McNab, J.A., Polimeni, J.R., Wang, R., Augustinack, J.C., Fujimoto, K., Stevens, A., Triantafyllou, C., Janssens, T., Farivar, R., Folkerth, R.D., Vanduffel, W., Wald, L.L., 2013. Surface based analysis of diffusion orientation for identifying architectonic domains in the in vivo human cortex. Neuroimage 69, 87–100.
Miller, K.L., Stagg, C.J., Douaud, G., Jbabdi, S., Smith, S.M., Behrens, T.E., Jenkinson, M., Chance, S.A., Esiri, M.M., Voets, N.L., Jenkinson, N., Aziz, T.Z., Turner, M.R., Johansen-Berg, H., McNab, J.A., 2011. Diffusion imaging of whole, post-mortem human brains on a clinical MRI scanner. Neuroimage 57, 167–181.
Van de Moortele, P.F., Auerbach, E.J., Olman, C., Yacoub, E., Ugurbil, K., Moeller, S., 2009. T1 weighted brain images at 7 Tesla unbiased for Proton Density, T2* contrast and RF coil receive B1 sensitivity with simultaneous vessel visualization. Neuroimage 46, 432–446.
Nagy, Z., Alexander, D.C., Thomas, D.L., Weiskopf, N., Sereno, M.I., 2013. Using high angular resolution diffusion imaging data to discriminate cortical regions. PLoS One 8, e63842.
Nie, J., Guo, L., Li, K., Wang, Y., Chen, G., Li, L., Chen, H., Deng, F., Jiang, X., Zhang, T., Huang, L., Faraco, C., Zhang, D., Guo, C., Yap, P.T., Hu, X., Li, G., Lv, J., Yuan, Y., Zhu, D., Han, J., Sabatinelli, D., Zhao, Q., Miller, L.S., Xu, B., Shen, P., Platt, S., Shen, D., Hu, X., Liu, T., 2012. Axonal fiber terminations concentrate on gyri. Cereb. Cortex 22, 2831–2839.
Nieuwenhuys, R., 2013. The myeloarchitectonic studies on the human cerebral cortex of the Vogt-Vogt school, and their significance for the interpretation of functional neuroimaging data. Brain Struct. Funct. 218, 303–352.
Peters, A., Sethares, C., 1996. Myelinated axons and the pyramidal cell modules in monkey primary visual cortex. J. Comp. Neurol. 365, 232–255.
Ramaswamy, S., Markram, H., 2015. Anatomy and physiology of the thick-tufted layer 5 pyramidal neuron. Front. Cell Neurosci. 9, 233.
Ronen, I., Ugurbil, K., Kim, D.S., 2005. How does DWI correlate with white matter structures? Magn. Reson Med. 54, 317–323.
Setsompop, K., Fan, Q., Stockmann, J., Bilgic, B., Huang, S., Cauley, S.F., Nummenmaa, A., Wang, F., Rathi, Y., Witzel, T., Wald, L.L., 2017. High-resolution in vivo diffusion imaging of the human brain with generalized slice dithered enhanced resolution: simultaneous multislice (gSlider-SMS). Magn. Reson Med.
Seunarine, K.K., Alexander, D.C., 2014. Multiple Fibers: beyond the Diffusion Tensor. Diffusion MRI, second ed. Academic Press, San Diego, pp. 105–123.
Smith, S.M., Beckmann, C.F., Andersson, J., Auerbach, E.J., Bijsterbosch, J., Douaud, G., Duff, E., Feinberg, D.A., Griffanti, L., Harms, M.P., Kelly, M., Laumann, T., Miller, K.L., Moeller, S., Petersen, S., Power, J., Salimi-Khorshidi, G., Snyder, A.Z., Vu, A.T., Woolrich, M.W., Xu, J., Yacoub, E., Ugurbil, K., Van Essen, D.C., Glasser, M.F., Consortium, W.U.-M.H., 2013. Resting-state fMRI in the human connectome Project. Neuroimage 80, 144–168.
Sotiropoulos, S.N., Jbabdi, S., Xu, J., Andersson, J.L., Moeller, S., Auerbach, E.J., Glasser, M.F., Hernandez, M., Sapiro, G., Jenkinson, M., Feinberg, D.A., Yacoub, E., Lenglet, C., Van Essen, D.C., Ugurbil, K., Behrens, T.E., Consortium, W.U.-M.H., 2013. Advances in diffusion MRI acquisition and processing in the human connectome Project. Neuroimage 80, 125–143.
Sotiropoulos, S.N., Hernandez-Fernandez, M., Vu, A.T., Andersson, J.L., Moeller, S., Yacoub, E., Lenglet, C., Ugurbil, K., Behrens, T.E., Jbabdi, S., 2016. Fusion in diffusion MRI for improved fibre orientation estimation: an application to the 3T and 7T data of the Human Connectome Project. Neuroimage 134, 396–409.
Thomas, C., Ye, F.Q., Irfanoglu, M.O., Modi, P., Saleem, K.S., Leopold, D.A., Pierpaoli, C., 2014. Anatomical accuracy of brain connections derived from diffusion MRI tractography is inherently limited. Proc. Natl. Acad. Sci. U. S. A. 111, 16574–16579.
Trampel, R., Bazin, P.L., Pine, K., Weiskopf, N., 2017. In-vivo magnetic resonance imaging (MRI) of laminae in the human cortex. Neuroimage.
Truong, T.K., Guidon, A., Song, A.W., 2014. Cortical depth dependence of the diffusion anisotropy in the human cortical gray matter in vivo. PLoS One 9, e91424.
Tuch, D.S., Reese, T.G., Wiegell, M.R., Makris, N., Belliveau, J.W., Wedeen, V.J., 2002. High angular resolution diffusion imaging reveals intravoxel white matter fiber heterogeneity. Magn. Reson Med. 48, 577–582.
Turner, R., Geyer, S., 2014. Introduction to the NeuroImage special issue: "In vivo Brodmann mapping of the human brain. Neuroimage 93 (Pt 2), 155–156.
Ugurbil, K., 2014. Magnetic resonance imaging at ultrahigh fields. IEEE Trans. Biomed. Eng. 61, 1364–1379.
Ugurbil, K., Xu, J., Auerbach, E.J., Moeller, S., Vu, A.T., Duarte-Carvajalino, J.M., Lenglet, C., Wu, X., Schmitter, S., Van de Moortele, P.F., Strupp, J., Sapiro, G., De Martino, F., Wang, D., Harel, N., Garwood, M., Chen, L., Feinberg, D.A., Smith, S.M., Miller, K.L., Sotiropoulos, S.N., Jbabdi, S., Andersson, J.L., Behrens, T.E., Glasser, M.F., Van Essen, D.C., Yacoub, E., Consortium, W.U.-M.H, 2013. Pushing spatial and temporal resolution for functional and diffusion MRI in the Human Connectome Project. Neuroimage 80, 80–104.
Vandevelde, I.L., Duckworth, E., Reep, R.L., 1996. Layer VII and the gray matter trajectories of corticocortical axons in rats. Anat. Embryol. Berl. 194, 581–593.
Vogt, O., 1903. Zur anatomischen Gliederung des Cortex cerebri. J. Psychol. Neurol. 2, 160–180.
Vogt, C., Vogt, O., 1919. Allgemeine Ergebnisse Unserer Hirnforschung.
Vu, A.T., Auerbach, E., Lenglet, C., Moeller, S., Sotiropoulos, S.N., Jbabdi, S., Andersson, J., Yacoub, E., Ugurbil, K., 2015. High resolution whole brain diffusion imaging at 7T for the Human Connectome Project. Neuroimage 122, 318–331.
Vu, A.T., Jamison, K., Glasser, M.F., Smith, S.M., Coalson, T., Moeller, S., Auerbach, E.J., Ugurbil, K., Yacoub, E., 2017. Tradeoffs in pushing the spatial resolution of fMRI for the 7T Human Connectome Project. Neuroimage 154, 23–32.
Waehnert, M.D., Dinse, J., Weiss, M., Streicher, M.N., Waehnert, P., Geyer, S., Turner, R., Bazin, P.L., 2014. Anatomically motivated modeling of cortical laminae. Neuroimage 93 (Pt 2), 210–220.
Waehnert, M.D., Dinse, J., Schafer, A., Geyer, S., Bazin, P.L., Turner, R., Tardif, C.L., 2016. A subject-specific framework for in vivo myeloarchitectonic analysis using high resolution quantitative MRI. Neuroimage 125, 94–107.
Wedeen, V.J., Hagmann, P., Tseng, W.Y., Reese, T.G., Weisskoff, R.M., 2005. Mapping complex tissue architecture with diffusion spectrum magnetic resonance imaging. Magn. Reson Med. 54, 1377–1386.
Wu, X., Auerbach, E., Vu, A.T., Moeller, S., Lenglet, C., Schmitter, S., Van de Moortele, P.F., Yacoub, E., Ugurbil, K., 2018. High resolution whole brain diffusion MRI at 7 Tesla using radiofrequency parallel transmission. Magn. Reson Med. 00, 1–14. https://doi.org/10.1002/mrm.27189.
Yeh, F.C., Verstynen, T.D., Wang, Y., Fernandez-Miranda, J.C., Tseng, W.Y., 2013. Deterministic diffusion fiber tracking improved by quantitative anisotropy. PLoS One 8 e80713.
Zhang, H., Schneider, T., Wheeler-Kingshott, C.A., Alexander, D.C., 2012. NODDI: practical in vivo neurite orientation dispersion and density imaging of the human brain. Neuroimage 61, 1000–1016.
Zhang, S., Cate, A.D., Herron, T.J., Kang, X., Yund, E.W., Bao, S., Woods, D.L., 2015. Functional and anatomical properties of human visual cortical fields. Vis. Res. 109, 107–121.